Profound seizure suppression and disease modification by targeting JAK1, a key driver of a pro-epileptogenic gene network.

Olivia R. Hoffman[1,2], Anna M. Patterson[1], Emily S. Gohar[1], Emanuel Coleman[3], Barry A. Schoenike[1], Claudia Espinosa-Garcia[4], Felipe Paredes[4], Raymond J. Dingledine[4], Jamie L. Maguire[3], Avtar S. Roopra[1,2]*

[1]Department of Neuroscience, University of Wisconsin-Madison School of Medicine and Public Health, Madison, WI 53705, USA; [2]Molecular and Cellular Pharmacology Graduate Program, University of Wisconsin-Madison School of Medicine and Public Health, Madison, WI 53705, USA; [3]Department of Neuroscience, Tufts University School of Medicine, Boston, MA 02111, USA; [4]Department of Pharmacology & Chemical Biology, Emory University School of Medicine, Atlanta, GA 30322, USA.

* asroopra@wisc.edu

ABSTRACT

Epilepsy is the 4th most prevalent neurological disorder with over 50 million cases worldwide. While a number of drugs exist to suppress seizures, approximately 1/3 of patients remain drug resistant, and no current treatments are disease modifying. Using network and systems-based approaches, we find that the histone methylase EZH2 suppresses epileptogenesis and slows disease progression, via repression of JAK1 and STAT3 signaling in hippocampal neurons. Pharmacological inhibition of JAK1 with the orally available, FDA - approved drug CP690550 (Tofacitinib) virtually eliminates behavioral and electrographic seizures after the onset of epilepsy in a preclinical rodent model of acquired epilepsy. Overall, identification of an endogenous protective response to status epilepticus in the form of EZH2 induction has highlighted a critical role for the JAK1 kinase in epilepsy. Targeting JAK1 with CP690550 has a profound therapeutic effect on spontaneous, recurrent seizures.

INTRODUCTION

Epilepsy is a highly prevalent neurological disorder with over 50 million cases worldwide[1,2]. Arising from a myriad of etiologies including gene mutations and environmental insults, the unifying characteristic of the epilepsies is the emergence of recurring, spontaneous seizures. Epileptogenesis is the process that links initial insults to the eventual propagation of spontaneous seizures. One of the insults that may initiate epileptogenesis is status epilepticus: an unremitting bout of seizures lasting for more than five minutes, during which the patient does not regain consciousness[3-5]. The first-line treatments for epilepsy are anticonvulsants aimed at controlling seizures. While these medications effectively suppress seizures for some patients, they do not target the processes that orchestrate progression of the disease, and fail to suppress seizures altogether in approximately 1/3 of patients[6]. There is a critical need for treatments that target the progressive decline in seizure threshold that arguably leads to spontaneous seizures.

A poor understanding of the mechanisms underlying epileptogenesis has so far prevented the development of disease biomarkers and translation of antiepileptogenic treatments from pre-clinical rodent models to the clinic. Although others have reported the disease-modifying potential of manipulations to metabolism[7-9], inflammation[10,11], chromatin modification[12], and signal transduction pathways[13], progress has been further hindered by a lack of consensus among laboratories employing different models of status epilepticus (SE)[14]. Finally, with few exceptions[7,15-18], little effort has been made to identify the principal transcription factors and chromatin modifiers whose function precipitates the gene changes that arise after status epilepticus.

Recently, we applied a systems approach and novel bioinformatic tool[19] to a transcriptomic consortium dataset that incorporated gene expression data across multiple laboratories and models of epilepsy[20]. This allowed for identification of potential mechanisms that span across rodent models of status epilepticus (SE) and human temporal lobe epilepsy (TLE)[21]. With this approach, we identified the histone methylase Enhancer of Zeste Homolog 2 (EZH2) as a potential driver of gene changes in dentate granule cells post-SE that is induced by an order of magnitude across epilepsy models. Transient pharmacological inhibition of EZH2 post-SE worsened epileptic phenotypes one month later, suggesting that EZH2 induction plays a protective role in

epileptogenesis. In addition to EZH2, our analysis predicted Signal Transducer and Activator of Transcription 3 (STAT3) to be a driver of gene activation across models of SE[20,21].

Of the studies that have profiled transcriptomic changes in the epileptic brain, nearly all find a robust induction of inflammatory pathways[15-18,21-23]. In the brain, inflammation can be triggered by glial cells[24], but neurons also exhibit an innate immune response that has been associated with hyper-excitability[25]. Anti-inflammatory drugs have been used with varying degrees of success to suppress seizures in human patients[26-29], and some drugs targeting neuroinflammation in rodents have shown antiepileptogenic potential[30-33]. However, the endogenous mechanisms that regulate neurogenic inflammation post-SE are poorly understood.

Herein, we show that EZH2 induction with SE suppresses pathological activation of the JAK/STAT pathway in neurons, a pathway commonly employed in inflammatory signaling. EZH2 deletion in neurons leads to hyper-activation of the JAK/STAT pathway, robust reductions in seizure threshold after SE, and an exaggerated epileptic phenotype. Pharmacological inhibition of JAK1/3 activity acutely after SE rescues these phenotypes. Finally, treatment with the JAK inhibitor CP690550 citrate after the onset of epilepsy profoundly suppresses spontaneous seizures.

RESULTS

EZH2 is robustly induced in hippocampal neurons across models of status epilepticus.

We previously identified the histone methyltransferase EZH2 as a potential driver of gene repression post-SE, and EZH2 protein was shown to be potently induced over a 10-day window post-SE in rats and mice across

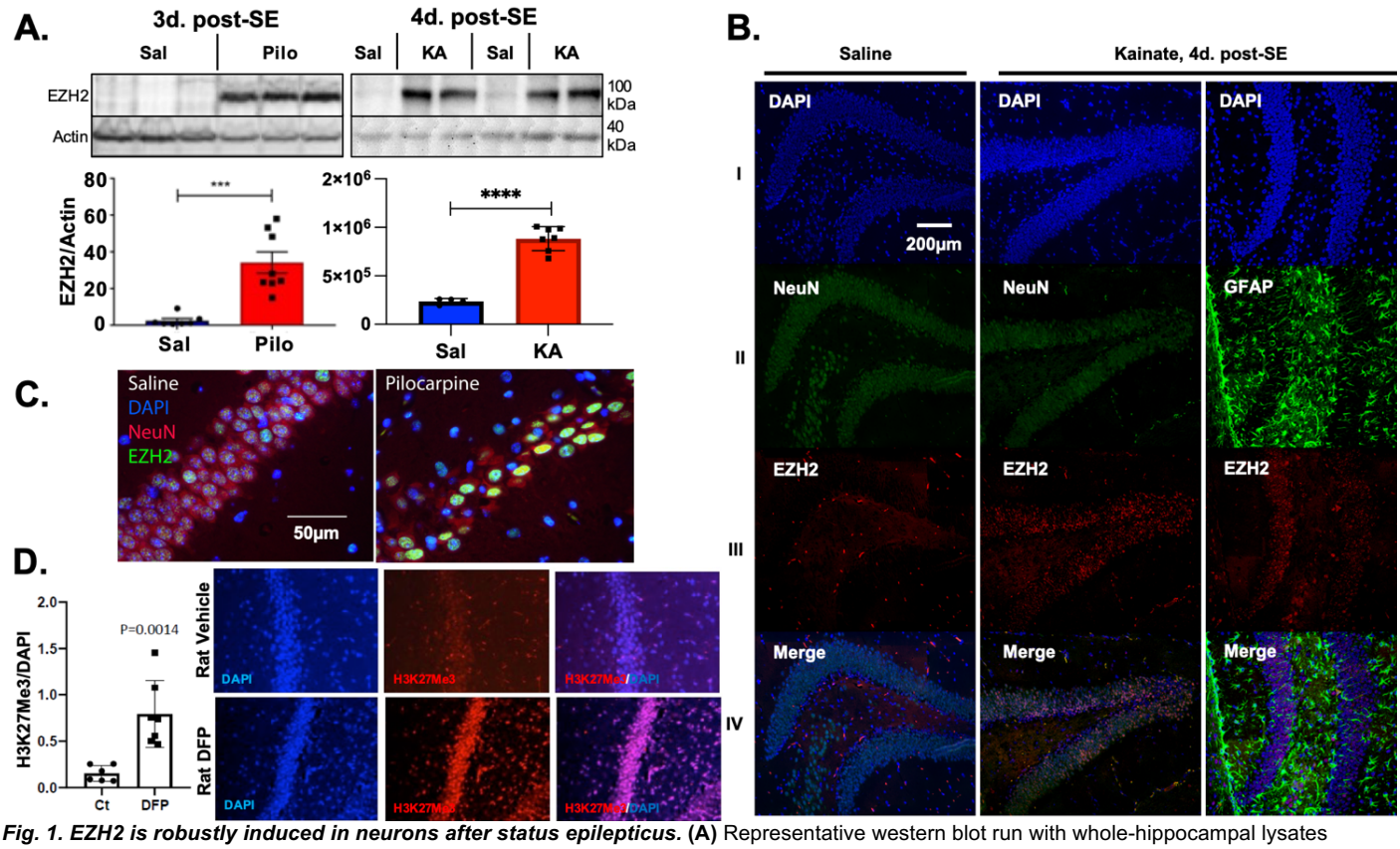

Fig. 1. EZH2 is robustly induced in neurons after status epilepticus. **(A)** Representative western blot run with whole-hippocampal lysates harvested on either day 3 post-SE from rats injected with pilocarpine (Pilo) and saline (Sal) or day 4 post-SE from C57BL6 mice injected (i.p.) with kainate (KA) and saline (Sal). All statistical analysis was performed by unpaired t-test. On day 3 post-SE, EZH2 is induced in C57BL6 mice injected with pilocarpine (pilo) by ~20 fold ($p<0.001$, n=7-8) over controls. KA mice exhibit a 3.7-fold induction of EZH2 over controls (t:10.03, $p<0.0001$, n=4-7). **(B)** Representative immunofluorescence images captured at 20x magnification on day 4 post-SE in Sal- and KA-treated mice were probed for DAPI (blue), GFAP/NeuN (green), and EZH2 (red). EZH2 is induced in kainate but not saline animals. EZH2-positive cells co-localize with the neuronal marker NeuN (see merged images). **(C)** EZH2 is induced in mouse CA1 pyramidal neurons day 3 post-pilo SE. **(D)** EZH2 methylase activity represented by H3K27Me3 (red) is probed alongside DAPI (blue) and in the dentate gyrus of hippocampi harvested from rats 3 days post-DFP or vehicle. H3K27Me3 is induced by 5-fold in DFP rats compared to controls ($p=0.0014$, n=6-7).

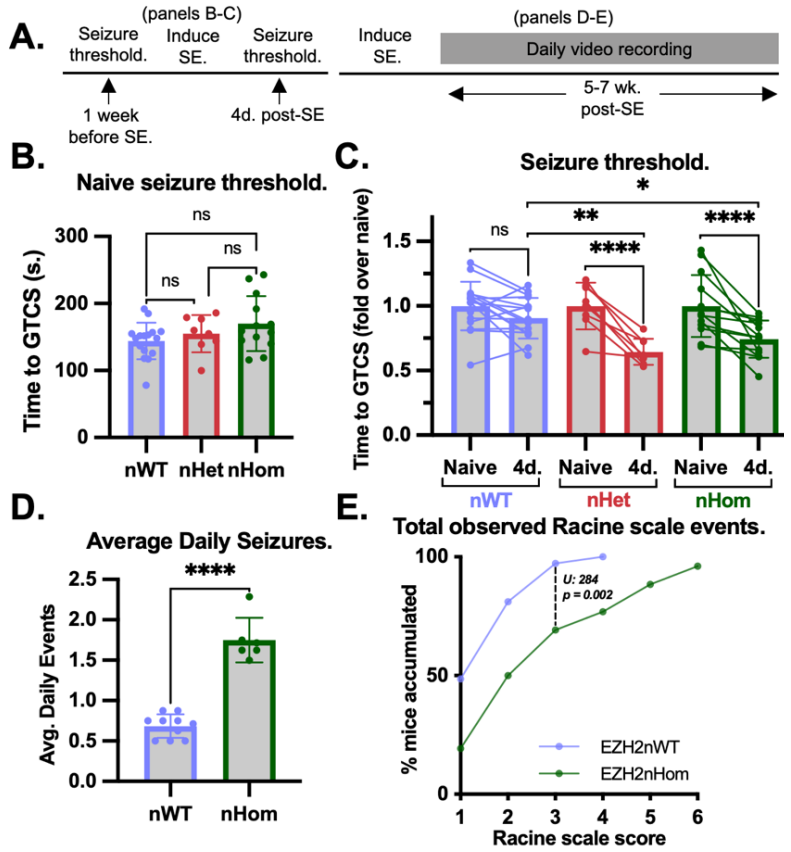

Fig. 2. EZH2 maintains seizure threshold after status epilepticus and mitigates spontaneous seizure frequency and severity. **(A)** Experimental paradigms for panels B-C and D-E. **(B)** Baseline fluorothyl seizure threshold data for C57BL6J EZH2nWT, nHet, and nHom mice. In naïve mice, deletion of EZH2 in neurons does not alter seizure threshold (nWT:nHet p=0.471, nWT:nHom p=0.134, nHet:nHom p=0.471). **(C)** After induction of SE by KA injection, seizure threshold does not change robustly in EZH2nWT mice (p=0.061). EZH2nHet mice exhibit a 35% reduction in seizure threshold post-SE (p<0.0001), with thresholds 25% lower than kainate-injected EZH2nWT mice (p=0.003). EZH2nHom mice show a 25% reduction in seizure threshold post-SE (p<0.0001), with thresholds 17% lower than KA EZH2nWT mice (p=0.026). Statistical analysis was performed using 2-way ANOVA with the Benjamini-Hochberg (B-H) correction for multiple comparison; n=7-14 mice per group. **(D)** FVB EZH2nWT and nHom mice were injected with KA to induce SE and video recorded from 5-7 weeks post-SE to count and score spontaneous seizure activity. Deletion of an EZH2 allele in neurons leads to a 2.5-fold increase in daily seizure events (p<0.0001). Results were analyzed by unpaired t-test (t: 10.20) (n=6-10 per group). **(E)** Total observed Racine scale events for EZH2nHom and EZH2nWT mice were quantified as a frequency distribution. 50% of EZH2nWT mice had only Class I seizures, while 50% of EZH2nHom mice had Class I and II seizures. Data was analyzed by Mann-Whitney test (U: 284, p=0.0024) (n=6-10 per group).

models of epilepsy[21]. To identify the cell types in which EZH2 induction occurs, hippocampi from mice 4 days post-SE were subjected to western blot analysis and immunofluorescence (IF). C57BL6 mice injected with kainate exhibit a 3.7-fold induction of EZH2 over controls, consistent with our observations in FVB mice[21] (Fig. 1A). Corroborating results of the western blots, there was strong EZH2 staining in NeuN-positive cells (Fig. 1B). Thus, EZH2 induction occurs in neurons post-SE. EZH2 is also robustly induced in mice 3 days after pilocarpine SE (Fig. 1A) in hippocampal principal neurons including CA1 pyramidal neurons (Fig. 1C). To test whether EZH2 is catalytically active after seizures, IF for H3K27 trimethylation (H3K27Me3) was performed on hippocampal sections from rats injected with vehicle or the chemoconvulsant diisopropylfluorophosphate (DFP) (Fig. 1D); H3K27Me3 was induced in the dentate gyrus after SE; similar results were obtained in the mouse pilocarpine model. These results show that EZH2 is robustly induced and catalytically active in neurons after status epilepticus in multiple models.

Neuronal EZH2 maintains seizure threshold and protects against exacerbated epileptic phenotypes.

To determine the role of EZH2 expression in epilepsy, we crossed EZH2 floxed mice[34] with Syapsin1 Cre drivers[35] to delete EZH2 in mature neurons. Neuronal specificity of Cre expression was confirmed via crossing Syn1Cre with *flox*-STOP-*flox*-tdTomato mice and immunofluorescence (Fig. S2A). Immunofluorescence and western blot analysis confirmed successful ablation of neuronal EZH2 post-SE. Fig. S2B-C show diminished induction of EZH2 on day 4 post-SE in mice lacking one EZH2 allele in neurons (EZH2nHet) or lacking both alleles (EZH2nHom). Staining for EZH2 confirmed reduced induction of neuronal EZH2 in EZH2nHet versus wildtype (EZH2nWT) mice (Fig. S2D, quantified in S2E).

We tested the impact of EZH2 deletion on fluorothyl seizure threshold acutely post-SE, as a correlation between fluorothyl seizure threshold[36] and the development of spontaneous seizures has been suggested[37-40]. We measured time to generalized tonic clonic seizure (GTCS) after exposure to the volatile chemoconvulsant fluorothyl in EZH2nWT, EZH2nHet, and EZH2nHom mice aged 4-6 weeks, before and after kainate-induced SE[41,42] (Fig. 2A). Loss of EZH2 alleles in neurons has no impact on seizure threshold in naïve mice (Fig. 2B), and induction of SE does not alter the seizure threshold of EZH2nWT mice on day 4 post-SE (Fig. 2C). In contrast, robust reductions in threshold were detected after SE in EZH2nHet mice (34%: mean difference: 55±8sec) and EZH2nHom mice (25%: mean difference: 46±8sec). These were significant reductions compared to EZH2nWT mice (2-way ANOVA; EZH2nHet: 28%, p=0.0036; EZH2nHom: 20%, p=0.0197). These data suggest that EZH2 is required to maintain fluorothyl seizure threshold post-SE.

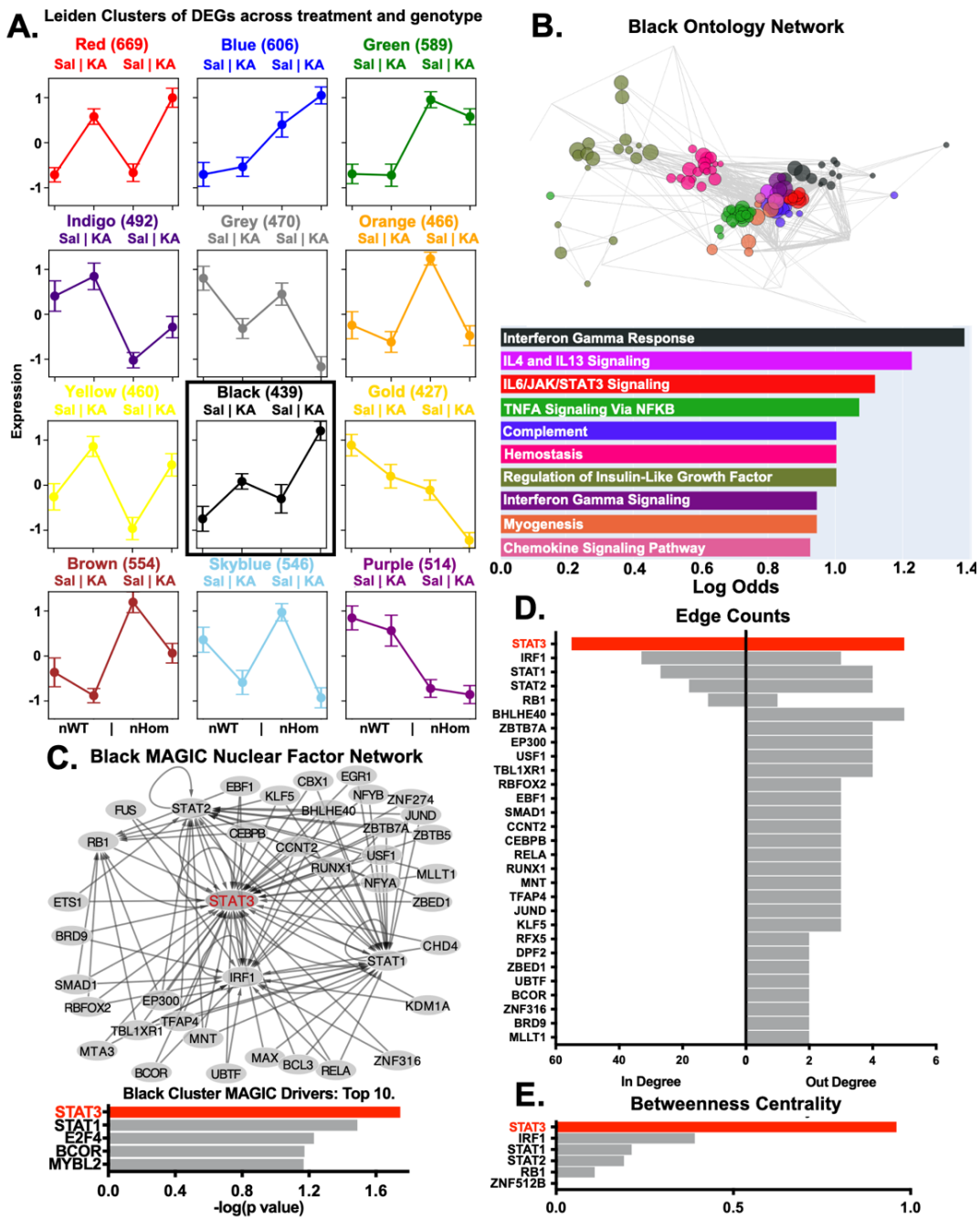

Fig. 3. STAT3 drives hyper-activation of pro-inflammatory networks post-SE in EZH2 knockout mice. **(A)** 6241 differentially expressed genes were identified through whole hippocampal RNAseq at an adjusted $p<10^{-2}$ across the four conditions (saline, kainate, EZH2nWT, and EZH2nHom) by Likelihood Ratio Test. A community-based approach grouped genes into clusters such that genes within a cluster behave similarly across the four conditions. Leiden clustering generated 13 distinct groups (violet group containing 8 genes not shown). The green, grey, orange, gold, brown, skyblue, and purple clusters are repressed after SE, whereas the red, blue, indigo, yellow, and black clusters are generally increased. The black cluster comprised 439 genes that were unchanged in naïve mice, and hyper-induced in EZH2nHom mice after SE. **(B)** Ontological analysis of genes in the black cluster. The 439 black cluster genes were compared to gene lists associated with terms in KEGG, Reactome, Biocarta, and Hallmark databases; terms with an odds ratio>1 and $p<0.05$ across all databases were projected as a network. **(C)** MAGIC was used to determine which Factors control the expression of black cluster genes, and positive hits were projected as a Gene Regulatory Network (GRN). Top 5 Factors driving expression in the black cluster are graphed below by –log(p value). STAT3 is the top factor. **(D)** Factors were ranked by their in degree count, out degree count, and **(E)** betweenness centrality.

We considered the possibility that EZH2 loss primed the mice to experience more severe responses to kainate injection, and it was this vulnerability to SE driving the observed reduction in mutant seizure threshold. However, we found no differences in time to first class V seizure and no correlation between time to first class V seizure and time to GTCS post-SE for either EZH2nWT (R^2:0.016, p=0.633), EZH2nHet (R^2:0.261, p=0.195), or EZH2nHom mice (R^2:0.152, p=0.209) (Fig. S3A-D).

To test the impact of neuronal EZH2 deletion on spontaneous seizures, we monitored behavioral spontaneous seizures in FVB EZH2nWT and EZH2nHom mice by video weeks five to seven post-SE (Fig. 2A). EZH2nHom mice exhibit a 2.5-fold increase in average daily seizure events compared to EZH2nWT mice (unpaired t-test; t:10.20, p<0.0001) (Fig. 2D). EZH2nHom mice also exhibit more severe Racine scale seizures than EZH2nWT mice (Mann Whitney test; U: 284, p=0.0024) (Fig. 2E). These data support the hypothesis that neuronal EZH2 induction is a protective response post-SE.

EZH2 tempers induction of the JAK/STAT pathway post-SE in neurons.

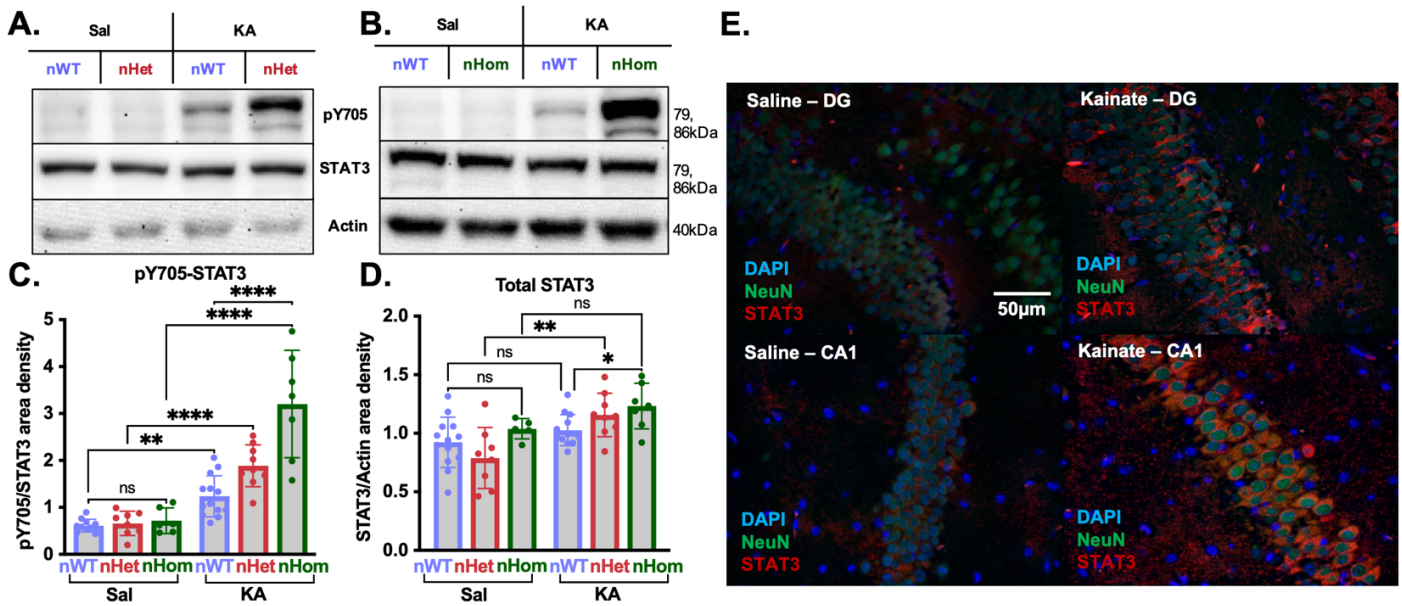

Fig. 4. JAK/STAT pathway components are hyper-activated in neurons of EZH2 knockout mice. EZH2nWT, nHet, and nHom mice were injected with saline or KA to induce SE; hippocampi were harvested on day 4 post-SE. **(A, B)** Representative western blots for pY705-STAT3, total STAT3, and beta-actin on day 4 post-SE. **(C)** pY705 levels are unchanged across genotypes in naïve animals (p=0.220). pY705 is induced by 2-fold in EZH2nWT mice (p=0.022), 2.9-fold in EZH2nHet mice (p<0.0001), and 4.5-fold in EZH2nHom mice post-SE (p<0.0001). pY705 levels in EZH2nHom mice post-SE are 2.6-fold greater than in EZH2nWT mice post-SE (p<0.0001). Results in panels C-D were analyzed by two-way ANOVA with the B-H correction for multiple comparisons (n=7-12). **(D)** Total STAT3 levels on day 4 post-SE. Total STAT3 is induced by 1.2-fold in nHom mice post-SE, compared to nWT mice post-SE (p=0.0407). Total STAT3 is induced after seizures in nHet mice by 1.5-fold (p=0.0407). **(E)** 40x images of the dentate gyrus (DG) and CA1 pyramidal cell layer (CA1). Hippocampal slices were collected on day 1 post-SE from saline- and KA-injected mice; immunofluorescence was performed to detect nuclear DNA, NeuN, and total STAT3.

To begin to understand the mechanism behind EZH2-mediated protection, we performed bulk RNAseq on whole hippocampal tissue from naïve and epileptic (4d. post-SE) EZH2nWT and EZH2nHom mice. Of the 10556 expressed genes, 6241 were found to be differentially expressed at an adjusted $p<10^{-2}$ (Likelihood Ratio Test) across the four conditions (saline, kainate, EZH2nWT, EZH2nHom). A community-based network approach was used to group genes into clusters. Leiden clustering generated 12 distinct groups (Fig. 3A). The green, grey, orange, gold, brown, skyblue, and purple clusters are generally repressed after SE, whereas the red, blue, indigo, yellow, and black clusters are generally increased. We focused on the black cluster because these 439 genes manifest induction with SE in EZH2nWT mice but show an exaggerated induction with SE in EZH2nHom mice. We reasoned that these would be genes whose expression is induced with SE but tempered in the presence of EZH2 post-SE and undergo unfettered induction in the absence of EZH2.

To understand the nature of genes comprising the black cluster, we performed an ontological analysis. The 439 Black cluster genes were compared to gene lists associated with terms in the KEGG, Reactome, Biocarta and Hallmark databases. (Fig. 2B). The ontology network highlights the innate immune response (NFkB, Interferon Gamma), microglial processes (Coagulation, ECM) and inflammation (IL6 Jak Stat3) amongst others. The term 'IL6 Jak Stat3' was of particular interest given that our previous work highlighted STAT3 as a driver of gene activation across models of epilepsy[21], and others have identified a role for the JAK/STAT pathway in epileptogenesis[25,30,43-46].

To determine which transcription factors and cofactors (hereafter together referred to as 'Factors') control expression of black cluster genes, we used MAGIC[19]. STAT3 was the highest scoring Factor (Fig. 3C). When projected as a Gene Regulatory Network (GRN) such that an arrow projects from Factor X to Factor Y if the gene encoding Factor Y is a transcriptional target of Factor X, STAT3 stands out as a central node. Thus, STAT3 has the highest indegree, outdegree and total edge count (Fig. 3D) of any Factor in the network. Finally, we assessed the Betweenness Centrality of the network[47] to determine which Factors might be critical for information flow in the GRN. STAT3 has by far the largest Betweenness Centrality of any Factor (Fig. 3E). Transient activation of the JAK/STAT pathway after SE has been reported by others[21,44] (and Fig. S4A-B). To test for a neuronal EZH2-dependent change in JAK/STAT signaling, we performed western blot analysis on hippocampal lysates from 4d. post-SE mice (Fig. 4A-B). On day 4 post-SE, pY705-STAT3 is induced 2-fold in

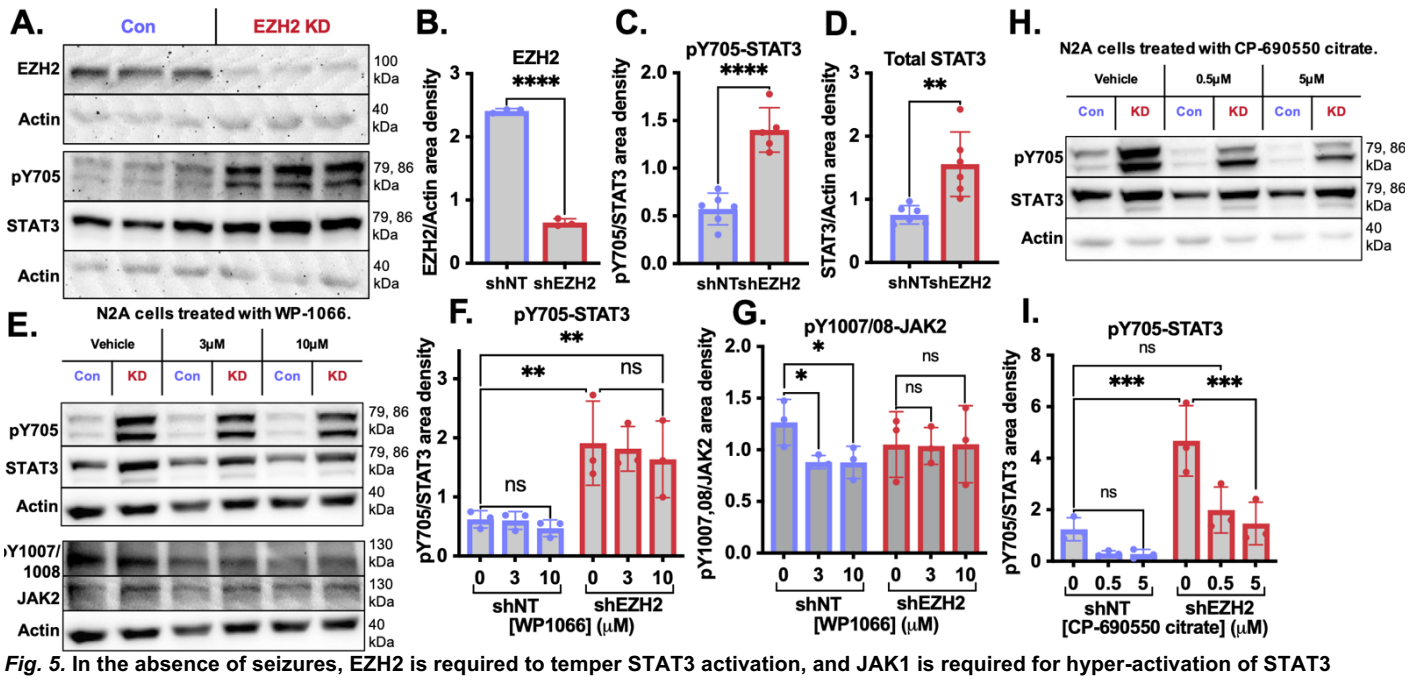

***Fig. 5.* In the absence of seizures, EZH2 is required to temper STAT3 activation, and JAK1 is required for hyper-activation of STAT3 downstream of EZH2.** N2A cells were stably transfected with EZH2 shRNA (shEZH2) or non-targeting shRNA (shNT). A 3.7-fold reduction in EZH2 protein in the knockdown cells was confirmed by western blot **(A-B)** ($p<0.0001$). We observe a 2.4-fold induction of pY705-STAT3 **(C)** in shEZH2 cells ($p<0.0001$). **(D)** Total STAT3 protein was induced by 2.1-fold in EZH2 KD cells ($p=0.004$). **(E)** shNT and shEZH2 cells were treated with the JAK2/STAT3 inhibitor WP1066 to a final concentration of 0 (DMSO), 3, or 10μM for one hour. Protein was harvested and subjected to western blot analysis. **(F)** Quantification of western blots in panel E. pY705-STAT3 is induced in vehicle-treated shEZH2 cells by 3-fold ($p=0.005$). WP1066 does not alter pY705 levels in control or knockdown cells at any concentration. **(G)** WP1066 reduces pY1007/08-JAK2 in shNT cells by 1.4-fold for both concentrations ($p=0.014$), but no change was observed in knockdown cells. **(H)** shNT and shEZH2 N2A cells were treated with the JAK inhibitor CP-690550 citrate to a final concentration of 0 (DMSO), 0.5, or 5μM for one hour. Protein was harvested and subjected to western blot analysis. **(I)** pY705-STAT3 is induced in vehicle-treated KD cells by 3.7-fold ($p=0.0004$). CP-690550 treatment reduces pY705-STAT3 levels of KD cells by 2.3-fold (at 0.5μM) and 3.2-fold ($p=0.0006$) (at 5μM). At 0.5μM CP, pY705 levels in KD cells are reduced to that of untreated control cells ($p=0.1804$). Results were analyzed by two-way ANOVA with the B-H correction for multiple comparisons; n=3 per group.

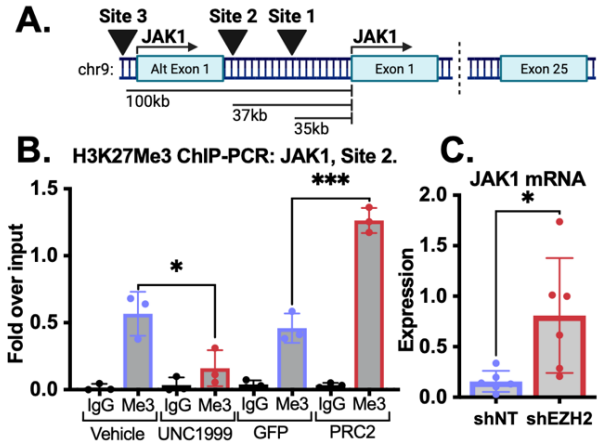

***Fig. 6. H3K27Me3 is enriched upstream of the JAK1 promoter.* (A)** Schematics depicting putative EZH2 binding sites on JAK1. **(B)** Parallel ChIP-qPCR experiments performed with antibodies against H3K27Me3, wherein N2A cells were treated with either vehicle or 10μM UNC1999 for 24 hours, or transfected with expression vectors for GFP-EZH2, SUZ12, and EED or GFP. qPCR was performed. Results were graphed as fold H3K27Me3 over input. Results were analyzed by unpaired t-test (n=3). For JAK1 (Site 2), treatment with UNC1999 reduces H3K27Me3 enrichment by 3.5-fold ($p=0.029$), and PRC2 overexpression leads to a 2.7-fold increase in H3K27Me3 enrichment ($p=0.0006$). **(C)** RT-PCR results for JAK1 mRNA expression in shNT and shEZH2 cells. JAK1 mRNA expression is induced by 5.1-fold in shEZH2 knockdown cells ($p=0.019$) (n=6).

EZH2nWT mice compared to naïve controls, 2.9-fold in EZH2nHet mice, and 4.5-fold in EZH2nHom mice (Fig. 4C-D). These results show an EZH2 gene dose-dependent hyperactivation of STAT3.

To determine the cell types in which STAT3 is expressed after seizures, we performed immunofluorescence with DAPI, NeuN, and total STAT3 antibodies on day 1 post-SE hippocampi taken from mice injected with saline or kainic acid (Fig 4E). We made use of the fact that the STAT3 gene is induced with STAT3 activation and so elevated total STAT3 protein is a proxy for activated STAT3. In both the dentate granule and CA1 pyramidal cell layer, we observed a robust induction of total STAT3 in NeuN-positive cells.

EZH2 targets STAT3 via JAK1 to suppress JAK/STAT signaling.

STAT3 is a central factor in the black GRN whereas, surprisingly, EZH2 is not. In order to understand how STAT3 hyperactivation can occur in the absence of EZH2, shRNA was used to knock down EZH2 in the Neuro2A (N2A) neuronal cell line. Fig. 5A shows a robust diminution of EZH2 in knockdown cells (EZH2 KD) (quantified in 5A,B) (3.7-fold, unpaired t-test; t:45.2, $p<0.0001$). This is associated with a marked increase in pY705-STAT3 levels (2.4-fold, unpaired t-test; $p<0.0001$) (Fig. 5A,C).

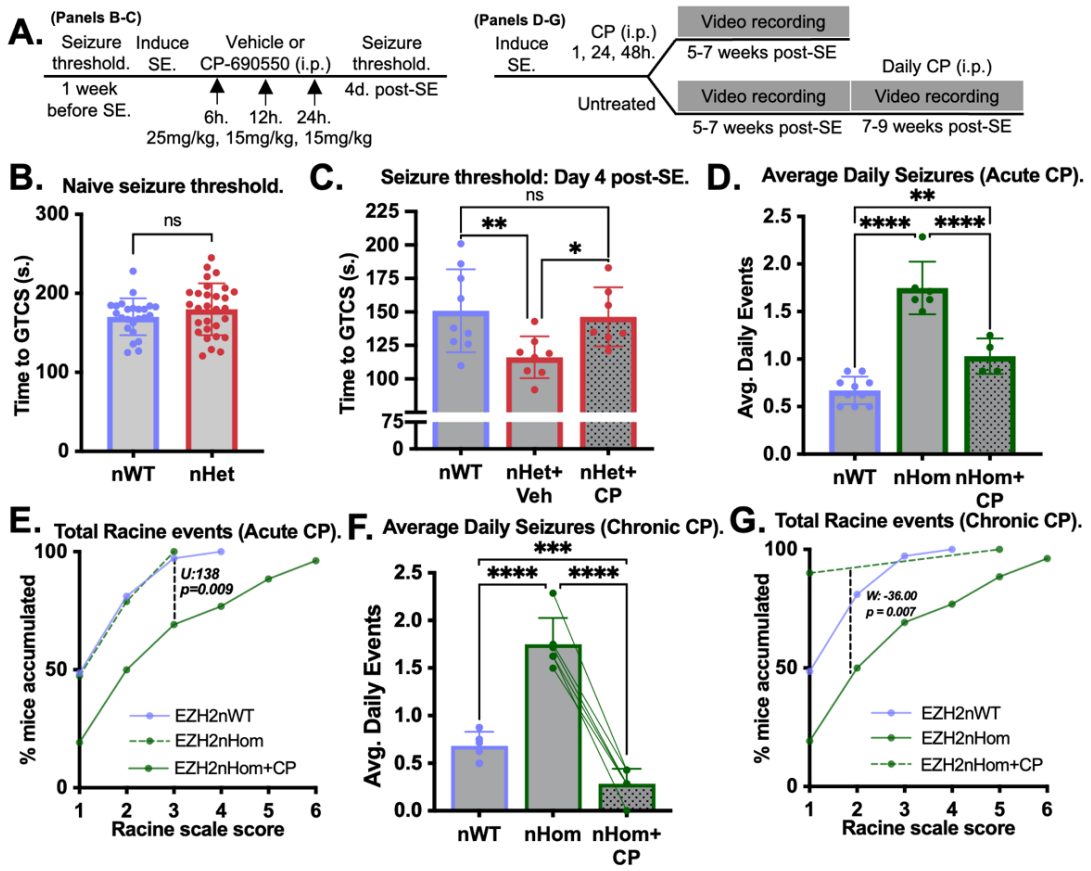

Fig. 7. JAK inhibition rescues seizure threshold reductions and spontaneous seizure burden in EZH2nKO mice. **(A)** (For panels B-C) Naïve seizure threshold was measured in C57 EZH2nWT and nHet mice one week prior to KA injections. **(B)** Deletion of an EZH2 allele does not alter seizure threshold in naïve mice (t:1.173, p=0.246, n=24-29). After SE, nHet mice were injected with vehicle or CP at 6, 12, and 24h. post-SE. **(C)** Seizure threshold was measured again on day 4 post-SE (n=7-9). Untreated nHet mice show a 35 second reduction in seizure threshold (p=0.007) compared to nWT mice. CP raises seizure thresholds of nHet mice by 30 seconds (p=0.025), extinguishing the difference between treated nHet and nWT mice (p=0.709). Results for panels C, D, and F were analyzed by one-way ANOVA with the B-H correction for multiple comparisons. In a parallel experiment, FVB EZH2nWT and nHom mice received CP or no treatment 1, 24, and 48h. post-SE, and SRS activity was monitored by video from 5-7 weeks post-SE (see panel A) (n=4-10). **(D)** nHom mice treated transiently with CP exhibit a 41% reduction in daily seizures compared to untreated nHom mice (p<0.0001); a 34% difference remains between treated nHom mice and nWT mice (p=0.0073). **(E)** Total observed Racine scale events were represented as a frequency distribution. Acute CP treatment reduces seizure severity in nHom mice (U:138.5, p=0.009) to nWT levels (U:357, p=0.955). 50% of nWT and treated nHom mice had Class I seizures, while 50% of untreated nHom mice had Class I and II seizures. Results were analyzed by Mann Whitney test. **(F)** SRS activity in untreated FVB nWT and nHom mice was monitored from 5-7 weeks post-SE, after which nHom mice received daily 10mg/kg CP injections during monitoring from 7-9 weeks post-SE (see panel A) (n=6-10). CP treatment in the chronic period reduced daily seizures by 80% in nHom mice (p<0.0001); treated nHom mice exhibit daily seizure frequencies 58% lower than that of nWT mice (p=0.0008). **(G)** Total observed Racine scale events were represented as a frequency distribution. Daily CP reduces seizure severity in nHom mice. 90th percentile seizure severities of nHom mice before and after treatment: 5.3 and 1, respectively (Wilcoxon matched pairs signed rank; W:-36.00, p=0.007). 90th percentile severity of WT mice: 2.6 (Mann Whitney test comparing nWT and treated nHom mice; U:119, p=0.042).

This result suggests EZH2 suppresses STAT3 activation in a cell-autonomous manner without circuit level alterations.

To determine whether STAT3-upstream kinases are required for pY705-STAT3 induction in EZH2 KD cell lines, we incubated cells with either WP1066 (an analogue of the JAK2 inhibitor AG490[48-50]) or CP690550 citrate (a small molecule inhibitor of JAK1/3 kinase activity[51-53]). WP1066 did not impact STAT3 phosphorylation in EZH2 KD cells at any concentration tested (Fig. 5F). In contrast, 500nM CP690550 citrate resulted in a 2.3-fold (p<0.01) reduction of pY705-STAT3 in EZH2 KD cells (Fig. 5H,I), rescuing pY705-STAT3 levels to that of vehicle-treated control cells. Even greater reduction occurred in the EZH2 KD cells treated with 5μM CP690550 (3.2-fold, p<0.001). CP690550 is a JAK inhibitor selective for JAK1 and JAK3, but JAK3 is not expressed in neurons or N2As (data not shown). Therefore, we hypothesize that EZH2 loss results in STAT3 activation via JAK1.

To understand how EZH2 regulates JAK1 activity, we noted three putative EZH2 binding sites in the gene body and promoter region of JAK1 using ENCODE tracks in the UCSC Genome Browser[54] (Fig. 6A, Fig. S6A). We performed chromatin immunoprecipitation with anti-H3K27Me3 antibodies to determine whether EZH2 methylase activity was enriched at any of these sites. Fig. 6B shows H3K27Me3 enrichment at site 2. Incubation of cells with UNC1999 (an EZH2 inhibitor[21,55]) for 24 hours resulted in a 3.5-fold loss of signal (unpaired t-test, p<0.05). Overexpression of EZH2, SUZ12, and EED (the core components of Polycomb) increased H3K27Me3 signal by 2.7-fold. Finally, RT-PCR on EZH2 knockdown cells showed a 5.1-fold induction of JAK1 mRNA over control cells (Fig. 6C) (unpaired t-test, p<0.05). PAX2 and actin were immunoprecipitated as positive and negative controls for H3K27Me3 enrichment, respectively (Fig. S6B-C);

Fig. S6D-G also depicts ChIP-PCR results for JAK1 (Site 1), JAK1 (Site 3), JAK2, and STAT3. None of these sites showed both a loss of H3K27Me3 enrichment after UNC1999 treatment and an increase in signal upon overexpression of Polycomb. These data are consistent with the hypothesis that EZH2 targets JAK1 transcription to temper activation of STAT3 in the absence of seizures. The data suggest that STAT3 hyperactivation upon loss of EZH2 can be suppressed with CP690550.

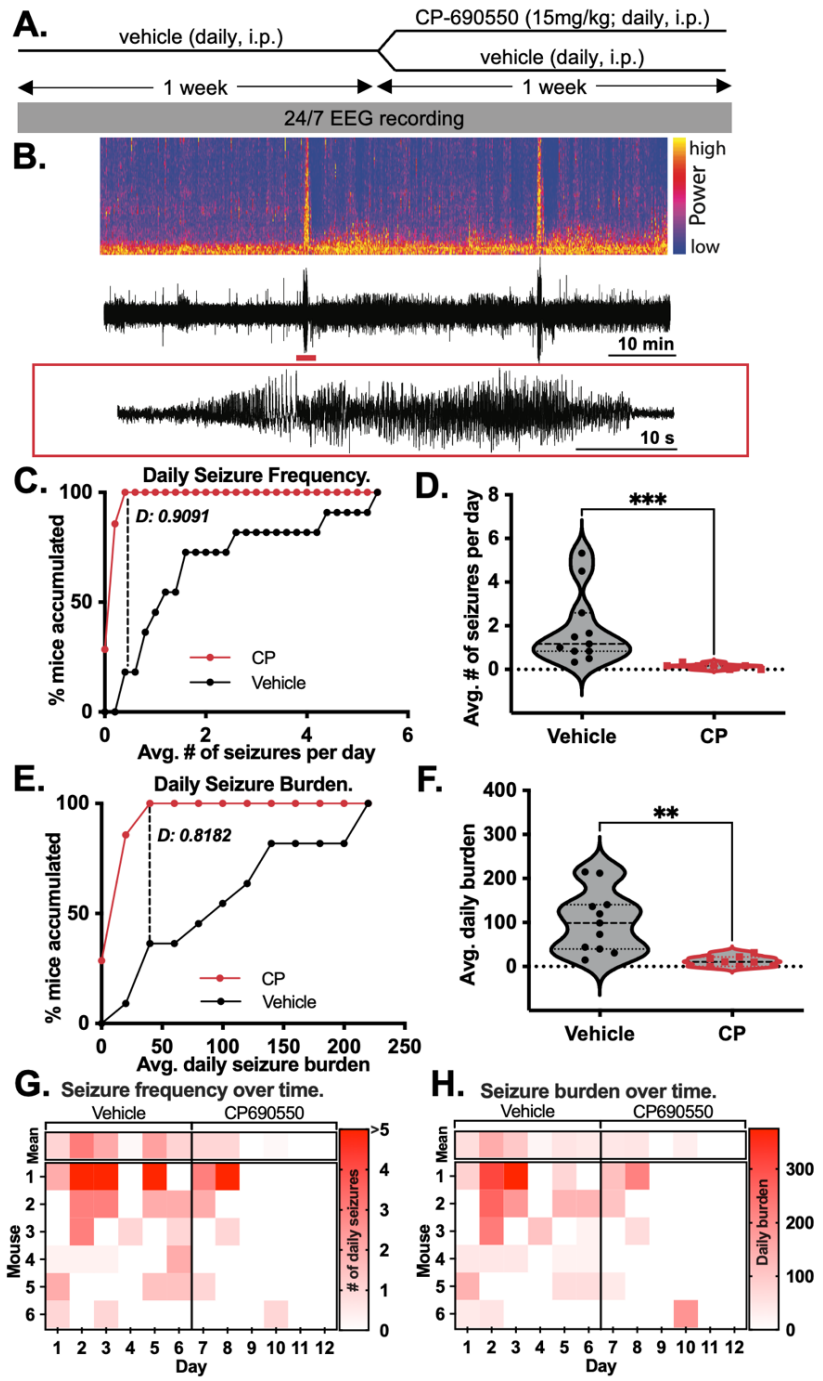

Fig 8. **CP profoundly suppresses spontaneous seizures in epileptic wildtype mice. (A)** SE was induced via IHKA, and mice equipped with EEG head mounts. All under continuous EEG recording, vehicle (i.p.) was administered daily for one week, followed by a week of daily vehicle or CP treatments (i.p., 15mg/kg). **(B)** Example power spectrum, trace, and seizure. Daily seizure frequency and burden were graphed as a cumulative frequency distribution **(C,E)** and violin plot **(D,F)** (grouped data). For cumulative graphs, bin centers are marked. 50% of vehicle-treated mice had up to 1.1 seizures per day on average, while 50% of CP-treated mice had <0.1 seizures per day on average. 100% of CP-treated animals had <0.4 seizures per day. 50% of untreated mice had up to 99 seconds of seizure burden per day, while 50% of treated mice had <11 seconds. 100% of treated mice had <40 seconds of seizure burden per day. **(G)** Paired seizure frequency of individual mice before and after CP treatment (n=6). With the exception of one seizure observed on day 10, CP treatment eliminated seizures for the last four days of treatment. **(H)** Paired seizure burden of individual mice before and after CP treatment. Analysis was performed on grouped data using the Kolmogorov-Smirnov test (**Frequency:** D:0.9091, p=0.0003; **Burden:** D:0.7083, p=0.0162) (n=7-12 per condition).

Transient JAK inhibition acutely post-SE rescues seizure threshold reductions in EZH2 knockout mice and stalls disease progression.

To test whether loss of EZH2-mediated regulation of JAK1 in neurons contributes to the exacerbated disease progression observed in EZH2 mutant mice, we treated EZH2nWT and EZH2nHet mice with CP690550 after induction of SE.

Because the hyper-induction of pY705-STAT3 in mutant mice occurs already at day 1 post SE (Fig. S7A-C), we injected mice with CP690550 or vehicle at 6, 12, and 24 hours post-SE. A cohort of mice was sacrificed three hours after final injection to assess hippocampal STAT3 activation by western blot (Fig. S7D). Treated mice exhibit a 2.6-fold reduction in pY705-STAT3 compared to untreated mice (Fig. S7E) confirming that CP690550 crosses the blood brain barrier to engage JAK signaling.

Consistent with the previous result (see Fig. 2B), neuronal deletion of EZH2 does not alter fluorothyl seizure threshold in naïve mice (Fig. 7B). CP690550 treatment raised the 4d. post-SE seizure threshold of EZH2nHet mice by 30 seconds (one-way ANOVA; p=0.025), rendering them indistinguishable from epileptic EZH2nWT mice (one-way ANOVA, p=0.709) (Fig. 7C). Thus, CP690550 rescued the increased seizure susceptibility phenotype associated with the loss of neuronal EZH2. These data support the hypothesis that EZH2 maintains seizure threshold post-SE by tempering activation of the JAK/STAT pathway.

To test whether transient CP690550 treatment immediately after SE mitigates long-term disease progression, mice were video recorded from weeks five to seven post-SE (Fig. 7A). CP690550 treatment immediately after SE reduces daily seizure frequency by 41% in EZH2nHom mice 5 weeks later (one-way ANOVA; $p<0.0001$). EZH2nHom seizure frequency was reduced from 2.6-fold above EZH2nWT to 1.5-fold (one-way ANOVA; $p=0.007$) (Fig. 7D). Along with a rescue of the seizure frequency phenotype, EZH2nHom mice treated acutely with CP690550 exhibited a dramatic reduction in seizure severity from untreated EZH2nHom mice (Mann-Whitney test; U: 138.5, $p=0.0091$), such that they were indistinguishable from WT mice (Fig. 7E).

To test whether CP690550 could rescue the increased seizure burden of EZH2nHom mice if administered during the chronic period, we recorded spontaneous seizures for two weeks post-SE in EZH2nWT and nHom mice, followed by another 2-week recording period during which the EZH2nHom mice received daily injections of CP690550 (Fig. 7A). Daily CP690550 treatment in the chronic period reduced seizure severity and frequency by 80% in EZH2nHom mice (one-way ANOVA; $p<0.0001$) (Fig. 7F-G). Indeed, seizure frequency of EZH2nHom+CP mice was reduced to below EZH2nWT levels (one-way ANOVA; 1.9-fold, $p=0.0008$).

CP690550 profoundly suppresses electrographic and behavioral spontaneous seizures in epileptic WT mice.

Given that chronic CP690550 treatment reduced seizure frequency of EZH2nHom mice to below WT levels, we tested its effect on WT epileptic mice. After the onset of spontaneous seizures, vehicle (i.p.) was administered daily for one week, followed by one week of daily vehicle or CP690550 injections (15mg/kg, i.p.), all under continuous EEG recording (Fig. 8A). Daily treatment for 1 week during the chronic period in WT mice profoundly suppressed spontaneous recurrent seizures. During vehicle treatment, 50% of mice had up to 1 seizure per day (Fig. 8C-D), with corresponding daily seizure burdens of up to 99 seconds (Fig. 8E-F). After CP690550 treatment, 50% of animals had <0.1 seizures per day, and <11 seconds of seizure activity per day. Further, whereas all animals experienced seizures during vehicle treatment, 30% experienced no seizures at all during CP690550 treatment. With the exception of one animal on day 3 of treatment, CP690550 eliminated seizures for all animals during the last four days of recording (Fig. 8G,H, Fig. S8A). Overall, CP690550 treatment robustly reduced spontaneous seizure frequency (Kolmogorov-Smirnov test; D:0.9091, $p=0.0003$) and seizure burden (D:0.8182, $p=0.0028$) in epileptic wildtype mice.

DISCUSSION

We have shown that STAT3 is a central node of an epileptic gene network and EZH2 exerts antiepileptogenic effects by antagonizing the JAK/STAT pathway. We provide evidence that the STAT3 upstream kinase JAK1 is a potent, novel therapeutic target for seizure suppression across epilepsy models and that it counteracts the process of epileptogenesis.

After status epilepticus, we find EZH2 protein is potently induced in hippocampal pyramidal and dentate granule neurons across models of epilepsy[21]. Additionally, EZH2 methylase activity is induced in the dentate gyrus after seizures (Fig. 1D). This comports with our identification of EZH2 as a potential driver of gene changes post-SE in rodents, and in human TLE[21]. Previously, we reported that treatment of mice with the SAM-competitive EZH2 inhibitor UNC-1999 exacerbated spontaneous seizures, and here we find that deletion of EZH2 in mature neurons has the same effect. Induction of Polycomb group (PcG) proteins has been studied in association with other brain insults. For example, sublethal ischemic insults lead to induction of PcG proteins in mouse cortical neurons, and in vitro
overexpression of PRC1 component BMI1 was sufficient to protect against oxygen-glucose deprivation-associated injury[56]. Further, sevoflurane (a volatile anesthetic that exerts positive allosteric modulation on $GABA_A$ receptors[57] and antagonizes NMDA receptors[58]) mediates the protective induction of EZH2 and H3K27Me3 to attenuate hypoxic-ischemic brain injury, reducing hippocampal autophagy and improving post-injury behavioral assessments in rats. Intriguingly, these improvements were reversed when rats treated with sevoflurane also received a dose of the EZH2 inhibitor GSK126[59]. These studies, along with our findings, point to a potentially general protective role for EZH2 in brain insults.

EZH2 deletion in neurons resulted in large transcriptomic changes that manifest after SE (Fig. 3). The black gene cluster housed genes whose expression were relatively unchanged in naïve EZH2nWT and EZH2nHom animals, induced after SE in EZH2nWT, and hyper-induced in EZH2nHom mice after SE. This pattern suggests that EZH2 might be responsible for tempering expression of genes in this cluster because its deletion resulted in their unfettered activation. The black cluster ontological analysis produced terms associated with innate immunity, neuroinflammation, and the JAK/STAT pathway. Network analysis placed STAT3 in the center of the black GRN and immunofluorescence confirmed induction of STAT3 in neurons post SE. While activation of the JAK/STAT pathway in non-neuronal cells post-SE is well-characterized[24,45,60,61], the role of STAT3 in neurons, especially in epilepsy has been less studied[43]. The mechanisms of neurogenic inflammation post-SE are not clear. Cytokines released from glial cells following seizures increase neuronal excitability[62], and type I IFNs increase excitability in neocortical pyramidal neurons via PKC[63]. Others have reported that seizure-induced activation of the JAK/STAT pathway reduces the number of gamma-aminobutyric acid (GABA) type A alpha1 receptors expressed in neurons following seizures, influencing GABA(A)R-dependent inhibition[25]; this group has also utilized pharmacological inhibition of STAT3[30] and genetic ablation of the STAT3 SH2 domain[43] to reduce spontaneous seizure frequency in rodent models of epilepsy. In summary, activation of neuroinflammatory pathways, including the JAK/STAT pathway, has been shown to modulate neuronal excitability, and herein we identify EZH2 as a key negative regulator of the JAK/STAT pathway in epileptogenesis.

We reasoned that hyper-induction of pY705-STAT3 post-SE in mutant mice might be a consequence of worsened disease progression more generally, rather than loss of EZH2 *per se*. To study the role of EZH2 in regulating the JAK/STAT pathway without the confounding variable of SE-related trauma and associated neuronal network activity, we developed an *in vitro* cell line model. Knocking down EZH2 in N2A cells results in induction of STAT3 Y705 phosphorylation. This activation was not via secretion of soluble factors as swapping media from control and knockdown cells failed to activate STAT3 (data not shown). WP1066, a JAK2 inhibitor[48-50] failed to suppress activated STAT3 in shEZH2 cells whereas CP690550 (a JAK1/3 inhibitor) did (Fig. 5H-I). Given that JAK3 is not expressed in these cells, we conclude that EZH2 tempers JAK1. Finally, we find that EZH2 directly interacts with the JAK1 locus (Fig. 6B). Increased activation of STAT3 at pY705-STAT3 as a result of EZH2 inactivation has also been observed in a transformed murine cell model of early T cell precursor acute lymphoblastic leukemia; EZH2 inactivation led to enrichment of documented STAT3 target genes, increased expression of IL6RA, and an exaggerated pY705-STAT3 induction in response to IL6 stimulation.[64] STAT-upstream receptors and kinases are also regulated by EZH2. In prostate cancer EZH2 directly targets the interferon gamma receptor gene INFGR1 to dampen JAK2/STAT1 signaling, and EZH2 depletion restores expression of IFN target genes as well as STAT1 phosphorylation.[65]

However, others have identified EZH2 as an activator of JAK/STAT signaling as well as a target of the pathway. When phosphorylated by AKT at serine 21, EZH2 disassociates from Polycomb to enhance STAT3 transcriptional activity through di-methylation of STAT3-K49 in glioblastoma cells[66-68]; we have performed western blotting to assess this posttranslational mark in mouse hippocampi post-SE and found no change in STAT3-K49Me2 after seizures or deletion of EZH2 (data not shown). Thus, this mechanism does not appear to play a role in N2As or the mouse brain. In NK/T-cell lymphoma, JAK3 phosphorylates EZH2 to mediate a switch in its function, promoting the transcriptional upregulation of oncogenes through the interaction of EZH2 and Pol-II[69]. To our knowledge, ours is the first report of EZH2 repressing JAK/STAT activation through JAK1.

EZH2nKO mice show both a decreased seizure threshold 4 days post SE as well as exaggerated seizure burden 5 weeks later compared to WT mice. CP690550 administration for 24 hours post-SE is sufficient to rescue both these phenotypes. This suggests that STAT3 hyper-induction is sufficient to explain both seizure threshold and burden in mutant mice. The observation that CP690550 profoundly suppresses spontaneous seizures when administered to EZH2nHom mice during the chronic period suggests ongoing, or reactivation of, JAK/STAT signaling during the chronic period (Fig. 7F-G, 8B-G). This supports the possibility that mechanisms involved in disease initiation (e.g., activation of neuroinflammatory pathways) continue to perpetuate disease chronically. Leveraging the brain's own protective mechanism, we used CP690550 to buttress EZH2 suppression of JAK1. CP690550 profoundly suppressed seizures in WT epileptic mice after two days of treatment. Whether cessation of CP690550 treatment leads to permanent disease-modifying effects, seizure relapse, or a compensatory reaction that worsens disease outcomes is the focus of future studies in the lab.

Anti-inflammatory drugs that have been used to suppress seizures in human patients[26-29] or have shown antiepileptogenic potential[30-33] in rodents pose several drawbacks: some or all are proposed only as supplemental therapies[26,27], risk worsened disease outcomes[27], show only transient effects[28], or are effective in only a subset of epilepsy patients[27,29]. We argue that an approach involving multiple animal models and multiple laboratories to identifying drivers of disease increases the likelihood of identifying druggable targets that are viable across etiologies. With this approach we identified EZH2 as a protective negative regulator of the JAK/STAT pathway in epilepsy. Our current data is consistent with the hypothesis that CP690550 mitigates spontaneous seizures in chronic epilepsy, and the cross-model approach by which we identified JAK1 and selected CP690550 suggests this drug may be useful across multiple epilepsies.

Recently, others have found that neuron-specific deletion of the STAT3 SH2 domain plateaued, but did not reduce, seizure frequency in chronic epilepsy[43], whereas CP690550 treatment eliminates seizures altogether. The explanation for this difference may be that there was incomplete ablation of STAT3 in their model, or it may suggest that the more robust therapeutic effect of CP690550 is attributable to JAK/STAT pathway suppression in non-neuronal cells (e.g., peripheral immune cells, microglia, etc.) as well as neurons.

The JAK/STAT pathway is likely one of many processes orchestrating disease progression. The data presented here represents the first evidence that EZH2 regulates JAK/STAT function through JAK1/STAT3 in epileptogenesis to reduce seizure burden. Transient treatment with CP690550 not only mitigates the effects of EZH2 deletion on seizure threshold acutely post-SE, but also exerts a lasting impact on disease progression in these mice. Furthermore, we find that intervention with CP690550 after the onset of spontaneous seizures not only rescues the effects of EZH2 deletion, but profoundly suppresses SRS in WT mice. These observations suggest an ongoing interplay between EZH2 and the JAK/STAT pathway. We conclude that EZH2-mediated tempering of the JAK/STAT pathway is required for maintaining seizure threshold post-SE, therein establishing a trajectory of epileptogenesis that impacts long-term disease outcomes.

METHODS

Bioinformatics

Reads were mapped to the mm39 build mouse genome and subjected to Likelihood Ratio Tests using Deseq2[70]. Transcripts per million were calculated and genes were classified as expressed if they had at least 3 TPM in all samples of any one of the 4 conditions (saline:WT, kainate:WT, saline:EZH2nHom, kainate:EZH2nHom). Deseq2 output was then filtered for only expressed genes and adjusted p-values were recalculated for the reduced number of genes. Genes with an adjusted p<.01 and 1.2-fold change were subjected to Leiden clustering with resolution=0.5 using the scanpy Leiden tool[71]. Ontology was performed on all clusters using Ontomancer (manuscript in preparation). Briefly, Biocarta, Hallmark, KEGG, and Reactome .gmt files were downloaded from https://www.gsea-msigdb.org/gsea/downloads.jsp. All databases were filtered for expressed genes and overlaps of cluster genes and gene sets associated with every term in Biocarta, Hallmark, KEGG, and Reactome databases were collected. For each cluster, Scores (S_t) for each term, t, were calculated as:

$$S_t = \sqrt{(\log\ O_t)^2 + {P_t}^2}$$

Where O_t and P_t, are the odds ratio and p values from Fisher exact tests. Only terms with O_t>1 and P_t<0.05 were kept for further analysis. For each term, a gene list is generated containing the overlap of genes in the cluster and term, G_t. A term x term similarity matrix was generated where similarity between term i and j is the Fisher exact test log odds ratio $O_{i,j}$ for the intersection of genes in the terms G_i and G_j. This was converted to a network where nodes are terms. Edge weights were calculated as:

$$weight = (\log(O_{i.j}) / \max \log O)^6$$

Where max log odds is the maximum log odds value across all comparisons. The 6 power was used to separate nodes for visualization. Networks were generated using the scanpy Leiden tool with resolution=2. Each community was named after the highest scoring term in that community.

MAGIC was performed on all clusters essentially as described[19] but with r=1, and GTFs were ignored. GTFs were defined as any ENCODE Factors containing the strings "TBP", "POL", "GTF", or "TAF".

Gene Regulatory Network was projected using Cytoscape[72] using MAGIC outputs. Factors were connected to their targets with edges defined as ChIP signal extracted from the Target Folder generated by MAGIC. Target genes of Factors that were not themselves Factors were removed to generate the GRN. Network statistics were calculated in Cytoscape[72].

Cell culture conditions, lentiviral knockdown, and PRC2 overexpression.

Cells were grown in 5% CO_2 at 37°C. Neuro2a cells were grown in MEM (#10-009-CV Corning, Manassas, VA) with 1.0g/L glucose, 1.5g/L L-Glutamine, and 10% fetal bovine serum (#26140-079 Gibco, Grand Island, NY). Stable EZH2 knockdown in Neuro2a cells for western blot and RNA analysis was achieved using SMARTvector lentiviral delivery of shRNA per the manufacturer instructions. Puromycin selection began 48 hours after infection and maintained during cell expansion and experimentation. SMARTvector lentiviral mouse EZH2 mEF1a-TurboRFP shRNA (#V3SM7592-232015353, Dharmacon, Lafayette, CO) targeted the sequence *ATCGTAGTAAGTACCAATG*, and non-targeting mEF1a-TurboRFP control particles (#S10-005000-01) were used as an infection control.

For overexpression of Polycomb, all plasmids were ordered and modified (if necessary) from Addgene (Watertown, MA). Control cells were transfected with pAdtrack-CMV (#16405). To overexpress PRC2, cells were transfected with pCMVHA-hEZH2 (#24230), pCMVHA-EED (#24231), and pCMVHA-SUZ12 (#24232). The EZH2 plasmid was modified in-house to produce an HA-EZH2-GFP fusion protein. All transfections were carried out with Lipofectamine 3000 transfection reagent (#L3000015, Invitrogen).

Animal care

All animal procedures and experiments were performed with approval from the University of Wisconsin-Madison School of Medicine and Public Health Instructional Animal Care and Use Committee, or the Institutional Animal Care and Use Committee of Emory University, as appropriate, and according to NIH national guidelines and policies.

Transgenic mice. Cre-driver and EZH2 floxed mice were ordered from Jackson Laboratories (#003966, #022616, Bar Harbor, ME). Mice were bred on a C57BL6 background. Using the previously described Synapsin1-Cre system [35] *EZH2*$^{+/-}$*; Syn1Cre*$^{+/-}$ (EZH2nHet) mice were generated by mating *EZH2*$^{flox/+}$*; Syn1Cre*$^{+/-}$ females with *EZH2*$^{flox/flox}$ and *EZH2*$^{flox/+}$ males [34]. *EZH2*$^{+/+}$*; Syn1Cre*$^{+/-}$ (EZH2nWT) mice were generated from mating pairs containing an *EZH2*$^{flox/+}$ male. To assess Cre expression, we used a reporter mouse with a lox-P flanked STOP cassette preventing transcription of tdTomato (#007909 Jackson Laboratories) [73]. Reporter males were bred with *Syn1Cre*$^{+/-}$ females to generate Cre-positive animals and Cre-negative controls.

Repeated low-dose KA model. Male and female C57BL6 and FVB mice were bred and housed under a 12-hour light/dark cycle with access to food and water *ad libitum*. C57BL6 mice were allowed to reach 4-6 weeks of age, and FVB animals 5-7 weeks of age, before undergoing experimentation. Kainate injections were performed at the same time of day (~10 A.M.), and mice were returned to home cages before the start of the dark cycle (~5 P.M.). Mice were housed with littermates for the duration of the experiment, with males and females separated at weaning.

We used a repeated low-dose kainate mouse model to induce SE. To begin, mice were weighed and singly housed in observation chambers for the duration of the injections. Mice were injected intraperitoneally (i.p.) with 5.0mg/kg synthetic kainic acid (KA) dissolved in 0.9% saline (#7065, Tocris Bioscience, Bristol, United Kingdom). At twenty-minute intervals, mice were given 5.0mg/kg injections of KA up to the third injection. The dosage was then reduced to 3.75mg/kg. Animals continued to receive 3.75mg/kg injections of KA every twenty minutes until each reached SE. The subsequent KA injection was skipped if an animal

experienced two or more Class V seizures within a single twenty-minute interval. Injections resumed for the next round, unless the animal reached SE. During induction of SE, seizures were scored using a modified Racine Scale [74] where I = freezing, behavioral arrest, staring spells; II = head nodding and facial twitches; III = forelimb clonus, whole-body jerks or twitches; IV = rearing; V = rearing and falling; VI = violent running or jumping behavior. Animals were considered to have reached SE after experiencing at least five Class V or VI seizures within a 90-minute window. KA mice were observed for 1-2 hours after SE. Animals were injected with 0.9% saline (s.c.), and soft gel food was provided in home cages. In the days following injection, animals were weighed and injected with 0.9% saline (s.c.) if body weight decreased by more than 0.5g.

Pilocarpine and DFP models of status epilepticus. Adult C57Bl/6 mice (8-12 weeks old, Charles River) were injected with terbutaline (4 mg/kg ip, Sigma T2528) and methylscopolamine (4 mg/kg ip, Sigma S8502) to alleviate respiratory and cardiovascular effects of pilocarpine, then 30 min later received saline or pilocarpine (280 mg/kg ip as free base, Sigma P6503) as described[32]. After 1 h of SE, seizures were interrupted by diazepam (10 mg/kg ip).

Adult male Sprague-Dawley rats (200-220 g, Charles River) were subjected to the DFP model of SE as described[33]. Briefly, rats received pyridostigmine bromide (0.1 mg/kg sc, TCI America, Portland, OR), followed 20 min later by atropine methylbromide (20 mg/kg sc, Sigma). After 10 min rats received saline (vehicle) or diisopropylfluorophosphate (DFP, 9.5 mg/kg ip, Sigma), and SE was allowed to abate naturally over 4-6 hr.

IHKA model of status epilepticus. The intrahippocampal kainic acid (IHKA) model was employed to generate chronically epileptic mice as previously described[75]. Kainic acid (100 nL of 20 mM; vIHKA) or vehicle (100 nL of sterile saline; vIHSA) was stereotaxically injected into the hippocampus using the following coordinate (from Bregma): 3.6 mm posterior, -2.8 mm lateral, and 2.8 mm depth. Only mice which experienced status epilepticus and went on to develop spontaneous recurrent seizures were used in the current study.

Fluorothyl seizure threshold testing. Male and female C57BL6 mice were bred and housed under a 12-hour light/dark cycle with access to food and water *ad libitum*. Animals were allowed to reach 4-6 weeks of age before undergoing experimentation. Fluorothyl seizure threshold tests were performed at the same time of day (~10 A.M.), and mice were returned to home cages before 5 P.M. Mice were housed with littermates for the duration of the experiment, with males and females separated at weaning. All seizure threshold tests were video recorded, and seizure behavior was scored by a blinded observer. Two tests per mouse were performed: the first at one week prior to kainate injections and the second at four days post-SE.

Seizure threshold tests were performed on male and female EZH2nWT wildtypes and EZH2nHet mutant mice using 100% bis(2,2,2-trifluoroethyl) ether (#287571, Sigma-Aldrich, St. Louis, MO). All tests were performed in a fume hood. Mice were placed in an airtight 10L. Plexiglas chamber (8.5”X10.75”X6.75”). Fluorothyl was infused into the chamber via a peristaltic pump at a rate of 40μL/minute onto a piece of Whatman filter paper placed at the top of the chamber. The time to generalized tonic clonic seizure (GTCS) was recorded from the start of fluorothyl infusion. Mice reached GTCS when they exhibited a complete loss of postural and motor control. After experiencing a generalized tonic clonic seizure, mice were rapidly removed from the chamber, and fluorothyl infusion was terminated. Mice were transferred to a recovery cage and kept isolated until motor control and normal behavior returned (~10 minutes). Mice were returned to home cages after recovery.

Long-term video monitoring for spontaneous seizures. Male and female FVB mice were bred and housed under a 12-hour light/dark cycle with access to food and water *ad libitum*. Animals were allowed to reach 5-7 weeks of age before undergoing experimentation. Video recording was performed at the same time of day (~10 A.M.), and mice were returned to home cages before 5 P.M. Mice were singly housed in chambers for the duration of recording with access to food and water. During daily CP690550 treatment, mice were weighed and injected daily before recording began. Videos were reviewed and scored by an experimenter blinded to treatment and genotype using the aforementioned modified Racine scale.

CP690550 citrate treatment of KA mice. Following kainate injections, an independent researcher (not the experimenter) randomly assigned mice to drug and vehicle conditions, and prepared both solutions. Drug and vehicle solutions were coded as “A” or “B.” CP690550 citrate (tofacitinib citrate) (#4556, Tocris Bioscience, Bristol, United Kingdom) was dissolved in a mixture of 70% saline (0.9%)/15% ethanol/15% DMSO. The 70% saline/15% ethanol/15% DMSO solution was administered as vehicle. The independent researcher provided

the blinded experimenter with the drug solutions and a list of all mice assigned to group A or B; this researcher did not participate in any seizure threshold testing or kainate injections. CP690550 or vehicle was delivered to mice intraperitoneally at 6, 12, and 24 hours post-SE. The drug doses for each of these time points, respectively, were 25mg/kg, 15mg/kg, and 15mg/kg.

Continuous EEG recording and seizure detection.
At the time of stereotaxic IHKA or IHSA injections, mice were implanted with chronic EEG recording headmounts (Pinnacle Technology, cat. #8201) which was affixed to the skull with 4 screws: 2 screws serving as EEG leads placed in the anterior and posterior cortex, 1 as a reference ground, and 1 as the animal ground. The headmounts were secured with dental cement. 24/7 EEG recordings were collected at 4 KHz using a 100X gain preamplifier high pass filtered at 1KHz (Pinnacle Technology, cat. #8292-SE) and tethered turnkey system (Pinnacle Technology, cat. #8200).

Seizures were detected using a custom analysis pipeline developed in-house in python (seizy; https://github.com/neurosimata/seizy) as previously described[75]. Briefly, EEG traces were automatically detected using a thresholding method from traces that were downsampled (decimated) to 100 Hz and divided into 5 second segments. Power (2-40 Hz) and line length were used to identify seizures. Seizures were only included if two consecutive 5 second segments were classified as seizures (minimum 10 seconds length) and were manually verified by an experienced investigator with expertise in electrographic seizure detection. Seizure frequency was calculated as the # of seizures per day by measuring total number of seizures a mouse had over a 24-hour period. The average seizure duration was calculated by taking the mean seizure duration for each mouse in each recording period. For each mouse, seizure burden was calculated as: (Total # of seizures * Average seizure duration)/(Total EEG recording hours).

Tissue isolation and homogenization

After KA seizure induction and/or treatment with CP690550 citrate, animals were sacrificed by rapid decapitation. Whole hippocampal hemispheres were harvested and flash-frozen in liquid nitrogen or on dry ice. Single hemispheres were lysed in Radioimmunoprecipitation Assay Buffer (RIPA: 50mM Tris, 150mM NaCl, 1% nonidet P-40, 0.5% sodium deoxycholate, 0.1% SDS) with mammalian protease inhibitor (1:1000, Sigma or 1860932 ThermoScientific) and phosphatase inhibitor (1:1000, Sigma or 78428 ThermoScientific). Protein from cell lines was harvested in Triton lysis buffer (3% 5M NaCl, 10% glycerol, 0.3% Triton X-100, 5% 1M Tris pH8.0) after PBS washes. Tissue was homogenized in lysis buffer by probe sonication (Fisher Scientific, Sonic Dismembrator, Model 100, Hampton, NH) on power 3 for two rounds, with 10 pulses per round. Supernatants were isolated by centrifugation and quantified using the DC Protein Assay (Bio-Rad, Hercules, CA) or BCA assay (ThermoScientific 23227). Protein extracts were stored at -80˚C. 5x loading buffer (0.5mM Tris, 10% SDS, 50% glycerol, 10mM EDTA, and 1% beta-mercaptoethanol) was added to each sample to reach a 1x final concentration. Extracts in loading buffer were boiled at 95˚C for 5 minutes and stored for up to one month at -20˚C until run on an acrylamide gel.

Western blotting

Protein extracts in loading buffer were loaded at 20µg per lane and resolved by electrophoresis in hand-poured acrylamide gels with a 5% acrylamide stacking layer (125mM Tris pH6.8, 5% acrylamide, 0.01% ammonium persulfate, 0.01% SDS, 0.01% TEMED) and an 8% acrylamide separating layer (375mM Tris pH8.8, 8% acrylamide, 0.015% ammonium persulfate, 0.015% SDS, 0.08% TEMED). Gels were transferred to polyvinyl difluoride membranes (PVDF; Millipore, Bedford, MA) using Tris-glycine transfer buffer (20mM Tris, 1.5M glycine, 20% methanol). Membranes were blocked with 5% bovine serum albumin (Fisher Scientific, Fair Lawn, NJ) diluted in low-salt Tris-buffered saline (w/w TBST; 20mM Tris pH7.5, 150mM NaCl, 0.1% Tween 20) with mammalian protease inhibitor (1:2000) and phosphatase inhibitor (1:2000), or Odyssey blocking solution (LI-COR, 927-60001) for 1 hour at room temperature. Primary antibodies were diluted in the same blocking buffer and incubated with membranes overnight at 4˚C. Antibodies include: EZH2 (1:1000, #5426 Cell Signaling, Danvers, MA), pY705-STAT3 (1:2000, #9145S Cell Signaling), STAT3 (1:1000, #12640 Cell Signaling), JAK2 (1:1000, #3230 Cell Signaling), JAK1 (1:1000, #3344S Cell Signaling), pY1034/35-JAK1 (1:1000, #74129S Cell Signaling), pY1007/08-JAK2 (1:500, ab32101, Abcam, Cambridge, UK), and Actin (1:10,000, #691001 MP Biomedicals) or GAPDH (1:10,000; Millipore, CB1001). The next day, the membranes were washed three times in 1X TBST and incubated with horseradish peroxidae-conjugated goat-anti-mouse

or -rabbit secondary antibodies for one hour at room temperature (1:10,000, Invitrogen #31430, #31460, Rockford, IL). Membranes were subsequently washed three times in TBST, and membranes were developed in SuperSignal West Femto ECL reagent (ThermoFisher, Waltham, MA). Bands were imaged using a ChemiDoc-It Imaging System (UVP Vision-Works, Upland, CA) and quantified using UVP Vision Works software or ImageJ. Band intensities were graphed and analyzed using Prism 9 software (GraphPad Software, La Jolla, CA).

RNA extraction and clean-up for whole hippocampal RNAseq

Hippocampi were harvested from saline- and kainate-treated EZH2nWT and EZH2nHom mice on day 4 post-SE (n=5 per treatment/genotype). RNA was extracted from hippocampal tissue with Trizol (#1559602, Life Technologies, Carlsbad, CA), and concentration was determined by spectrometry. This was followed by a treatment with DNase (#AM2238, Invitrogen). Finally RNA clean-up was carried with the RNeasy Mini Kit (#74104, Qiagen, Hilden, Germany). Purified samples were submitted to the Gene Expression core at the University of Wisconsin-Madison Biotechnology Center for library preparation and sequencing (https://biotech.wisc.edu).

Chromatin immunoprecipitation and qPCR.

4% formaldehyde was used to crosslink proteins to chromatin before neutralization of the reaction in 125mM glycine, and washes in 1X PBS (pH 7.4). Chromatin was fragmented in Triton-X lysis buffer and 1:100 protease inhibitors; lysates were sonicated and centrifuged to remove cell debris. Protein concentration of the supernatant was quantified with BioRad Bradford assay reagent (#5000006). Chromatin was incubated overnight at 4 degrees Celsius with antibodies against H3K27Me3 (#9733 Cell Signaling) or rabbit IgG. The next day, protein A/G magnetic beads (#88803, ThermoScientific) were blocked in BSA and salmon sperm DNA while chromatin samples were centrifuged, after which chromatin-antibody complexes were added to the beads to incubate. Washes were performed in a low-salt ChIP buffer (1% SDS, 1% Triton X-100, 0.4% 500mM EDTA, 2% 1M Tris pH8.1, 3% 5M NaCl). Decrosslinking buffer (1% SDS, 100mM $NaHCO_3$, 200mM NaCl) was then added to IgG samples, H3K27Me3 samples, and inputs; decrosslinking reactions were allowed to incubate overnight in a 65 degree Celsius water bath. Phenol-choloform DNA extraction was performed the next day. Quantitative PCR was performed with 2x SYBR green mix (#RR420L, Takara Bio, Otsu, Shiga, Japan) and primers against JAK1, STAT3, JAK2, PAX2, Hoxc10, and beta actin (primers listed at the end of the methods section). Signal was calculated from standard curves generated by serial dilution of an input sample, and enrichment values were expressed as fold over input. RNA for RT-PCR was extracted with Trizol, and concentration was determined by spectrometry. PCR reactions were run with primers against JAK1 and GAPDH. cDNA synthesis was run on the MJ Mini Thermocycler from Bio-Rad, and PCR reactions were run on the MJ Research DNA Engine Opticon 2 Continuous Fluorescence Detector using Opticon Monitor software.

Immunofluorescence

Whole brains were harvested on day 3 or 4 post-SE, bisected sagitally, fixed in 4% paraformaldehyde, dehydrated in a series of graded TBS-Tween/ethanol solutions, embedded in paraffin, sectioned at 5μm and subjected to immunofluorescence for EZH2, H3K27me3, NeuN, GFAP, total STAT3, and DAPI. Heat induced antigen retrieval was performed in a 10mM citric acid buffer (pH 6.0). After a blocking step, rabbit anti-EZH2 (1:50) (#5246 Cell Signaling), rabbit anti-H3K27me3 (1:300) (#39155 Active Motif), mouse anti-NeuN (1:200 ab104224 Abcam, or 1:500 MAB377 from Millipore) primary antibodies were applied and incubated overnight at 4°C. Slides were washed with PBS then incubated with goat-anti-mouse or goat-anti-rabbit Alexa Fluor 488 (ab150113 Abcam or A11005, A11008 from InVitrogen, respectively) and goat-anti-rabbit Alexa Fluor 594 (ab150080 Abcam or Jackson ImmunoResearch) secondary antibodies at a concentration of 1:200 for one or two hours at room temperature, followed in some experiments by two-hour incubation at room temperature with Alexa Fluro 488-conjugated mouse anti-GFAP antibody (1:200) (#53-9892-82 Invitrogen). Nuclear DNA was stained with DAPI (300 nM) or a DAPI-containing mounting media (#H-1200 Vector Laboratories, Burlingame, CA). Slides were imaged at 20-40x magnification using a fluorescent microscope (Nikon E600 microscope with fluorescence or Zeiss Axio Observer A1 epifluorescence microscope). Images were captured with Zeiss Axiovision or Cellsens software (Olympus Life Science Solutions, Center Valley, PA). Image

analysis and quantification was performed in ImageJ (NIH, https://imagej.nih.gov/ij/). EZH2 antibody specificity was confirmed before usage, as shown in Fig. S1A.

Statistical analysis

For all statistical analysis – with the exception of RNAseq data – FDR < 0.05 corrected for multiple comparisons was considered statistically significant. Data were graphed as mean ± standard error of the mean (SEM) in Prism 9 software (Graphpad Software, La Jolla, CA). Statistical tests were also performed in Prism. Western blot, seizure threshold, and spontaneous seizure data was analyzed by 2-way or 1-way ANOVA with the Benjamini-Hochberg FDR method for multiple comparisons, or by unpaired t-test where appropriate.

Primer List
mouse-JAK1-Site1 (ChIP):
(forward) *CTCTGCTCGCTTTCCCGGAGATGC*
(reverse) *CTCGGAGGCTGGAGCGTGACTTCT*

mouse-JAK1-Site2 (ChIP):
(forward) *TGACTCGCACCCAGCCTGAAATGG*
(reverse) *GCGGCCCAGTCACCCGAAGAAATA*

mouse-JAK1-Site3 (ChIP):
(forward) *TTCGCGGGGCAAGGGAAAGGATTC*
(reverse) *CCACCGCTCAGGGCTCTGGGTTTT*

mouse-JAK2 (ChIP):
(forward) *CGCCGCTGCGGGATGTGAGTGC*
(reverse) *GGAGGCGGGATCGCAGGGAGAACC*

mouse-STAT3 (ChIP):
(forward) *CGGGCGAGCGCTGTACTTCCTA*
(reverse) *AAGCGAGCCGTATCAGGGCATTTA*

mouse-PAX2 (ChIP):
(forward) *GCGGCGCTCAGTCGCGTTCATAG*
(reverse) *CTCCCCGGAGTCTGGGCAGTCCA*

mouse-Hoxc10 (ChIP):
(forward) *GCGGGGGCCCTCTGCCTAAT*
(reverse) *CCCGGCCCTGGGCTCACACT*

mouse-JAK1 (RT-PCR):
(forward) *GCGCCCAGCCTCGCTCGTC*
(reverse) *AACGCCATGGCATTGCAGTCCTCT*

mouse-GAPDH (RT-PCR):
(forward) *ACGGCAAATTCAACGGCACAGTCA*
(reverse) *TGGGGGCATCGGCAGAAGG*

Funding. Supported by CURE (AR), Lily's Fund (AR), NIH grant 1R01NS108756 (AR, RD) and R01NS105628, R01NS102937, and R21NS120868 (JM).

Acknowledgements. We thank Asheebo Rojas for providing rat brain tissues in the DFP model.

Conflict of Interest. JM serves on the Scientific Advisory Board and has a Sponsored Research Agreement with SAGE Therapeutics for work unrelated to this project. AR and RD have no conflicts of interest to declare.

References

1 Hirtz, D. *et al.* How common are the "common" neurologic disorders? *Neurology* **68**, 326 (2007). https://doi.org/10.1212/01.wnl.0000252807.38124.a3

2 Gavvala, J. R. & Schuele, S. U. New-Onset Seizure in Adults and Adolescents: A Review. *Jama* **316**, 2657 (2016). https://doi.org/10.1001/jama.2016.18625

3 French, J. A. *et al.* Characteristics of medial temporal lobe epilepsy: I. Results of history and physical examination. *Annals of Neurology* **34**, 774 (1993). https://doi.org/10.1002/ana.410340604

4 Trinka, E. *et al.* A definition and classification of status epilepticus--Report of the ILAE Task Force on Classification of Status Epilepticus. *Epilepsia* **56**, 1515 (2015). https://doi.org/10.1111/epi.13121

5 Hesdorffer, D. C., Logroscino, G., Cascino, G., Annegers, J. F. & Hauser, W. A. Risk of unprovoked seizure after acute symptomatic seizure: effect of status epilepticus. *Annals of Neurology* **44**, 908 (1998). https://doi.org/10.1002/ana.410440609

6 Sankaraneni, R. & Lachhwani, D. Antiepileptic drugs--a review. *Pediatric Annals* **44**, e36 (2015). https://doi.org/10.3928/00904481-20150203-10

7 Garriga-Canut, M. *et al.* 2-deoxy-D-glucose reduces epilepsy progression by NRSF-CtBP-dependent metabolic regulation of chromatin structure. *Nature Neuroscience* **9**, 1382-1387 (2006). https://doi.org/10.1038/nn1791

8 Stafstrom, C. E., Roopra, A. & Sutula, T. P. Seizure suppression via glycolysis inhibition with 2-deoxy-D-glucose (2DG). *Epilepsia* **49 Suppl 8**, 97 (2008). https://doi.org/10.1111/j.1528-1167.2008.01848.x

9 Stafstrom, C. E. *et al.* Anticonvulsant and antiepileptic actions of 2-deoxy-D-glucose in epilepsy models. *Annals of Neurology* **65**, 435 (2009). https://doi.org/10.1002/ana.21603

10 Vezzani, A., Friedman, A. & Dingledine, R. J. The role of inflammation in epileptogenesis. *Neuropharmacology* **69**, 16 (2013). https://doi.org/10.1016/j.neuropharm.2012.04.004

11 Rojas, A. *et al.* A Novel Second-Generation EP2 Receptor Antagonist Reduces Neuroinflammation and Gliosis After Status Epilepticus in Rats. *Neurotherapeutics: The Journal of the American Society for Experimental NeuroTherapeutics* (2021). https://doi.org/10.1007/s13311-020-00969-5

12 Williams-Karnesky, R. L. *et al.* Epigenetic changes induced by adenosine augmentation therapy prevent epileptogenesis. *Journal of Clinical Investigation* **123**, 3552-3563 (2013). https://doi.org/10.1172/jci65636

13 Liu, G. *et al.* Transient inhibition of TrkB kinase after status epilepticus prevents development of temporal lobe epilepsy. *Neuron* **79**, 31 (2013). https://doi.org/10.1016/j.neuron.2013.04.027

14 Landis, S. C. *et al.* A call for transparent reporting to optimize the predictive value of preclinical research. *Nature* **490**, 187 (2012). https://doi.org/10.1038/nature11556

15 Becker, A. J. *et al.* Correlated stage- and subfield-associated hippocampal gene expression patterns in experimental and human temporal lobe epilepsy. *The European Journal of Neuroscience* **18**, 2792 (2003). https://doi.org/10.1111/j.1460-9568.2003.02993.x

16 Borges, K., Shaw, R. & Dingledine, R. Gene expression changes after seizure preconditioning in the three major hippocampal cell layers. *Neurobiology of Disease* **26**, 66 (2007). https://doi.org/10.1016/j.nbd.2006.12.001

17 Hansen, K. F., Sakamoto, K., Pelz, C., Impey, S. & Obrietan, K. Profiling status epilepticus-induced changes in hippocampal RNA expression using high-throughput RNA sequencing. *Scientific Reports* **4** (2014). https://doi.org/10.1038/srep06930

18 McClelland, S. *et al.* The transcription factor NRSF contributes to epileptogenesis by selective repression of a subset of target genes. *eLife* **3** (2014). https://doi.org/10.7554/eLife.01267

19 Roopra, A. MAGIC: A tool for predicting transcription factors and cofactors driving gene sets using ENCODE data. *PLoS computational biology* **16** (2020). https://doi.org/10.1371/journal.pcbi.1007800

20 Dingledine, R. *et al.* Transcriptional profile of hippocampal dentate granule cells in four rat epilepsy models. *Scientific Data* **4** (2017). https://doi.org/10.1038/sdata.2017.61

21 Khan, N. *et al.* A systems approach identifies Enhancer of Zeste Homolog 2 (EZH2) as a protective factor in epilepsy. *Plos One* **14** (2019). https://doi.org/10.1371/journal.pone.0226733

22 Pfisterer, U. *et al.* Identification of epilepsy-associated neuronal subtypes and gene expression underlying epileptogenesis. *Nature Communications* **11** (2020). https://doi.org/10.1038/s41467-020-18752-7

23 Cid, E. *et al.* Sublayer- and cell-type-specific neurodegenerative transcriptional trajectories in hippocampal sclerosis. *Cell Reports* **35** (2021). https://doi.org/10.1016/j.celrep.2021.109229

24 Kumar, P. *et al.* Single-cell transcriptomics and surface epitope detection in human brain epileptic lesions identifies pro-inflammatory signaling. *Nature Neuroscience* **25**, 956 (2022). https://doi.org/10.1038/s41593-022-01095-5
25 Lund, I. V. *et al.* BDNF Selectively Regulates GABAA Receptor Transcription by Activation of the JAK/STAT Pathway. *Science Signaling* **1**, ra9 (2008). https://doi.org/10.1126/scisignal.1162396
26 You, S. J., Jung, D. E., Kim, H. D., Lee, H. S. & Kang, H. C. Efficacy and prognosis of a short course of prednisolone therapy for pediatric epilepsy. *European journal of paediatric neurology: EJPN: official journal of the European Paediatric Neurology Society* **12**, 314 (2008). https://doi.org/10.1016/j.ejpn.2007.09.003
27 Dubey, D. *et al.* Randomized Placebo-Controlled Trial of Intravenous Immunoglobulin in Autoimmune LGI1/CASPR2 Epilepsy. *Annals of Neurology* **87**, 313 (2020). https://doi.org/10.1002/ana.25655
28 Gayatri, N. A., Ferrie, C. D. & Cross, H. Corticosteroids including ACTH for childhood epilepsy other than epileptic spasms. *The Cochrane Database of Systematic Reviews* (2007). https://doi.org/10.1002/14651858.CD005222.pub2
29 Lai, Y.-C. *et al.* Anakinra usage in febrile infection related epilepsy syndrome: an international cohort. *Annals of Clinical and Translational Neurology* **7**, 2467 (2020). https://doi.org/10.1002/acn3.51229
30 Grabenstatter, H. L. *et al.* The effect of STAT3 inhibition on status epilepticus and subsequent spontaneous seizures in the pilocarpine model of acquired epilepsy. *Neurobiology of Disease* **62**, 73 (2014). https://doi.org/10.1016/j.nbd.2013.09.003
31 Jiang, J. *et al.* Suppressing pro-inflammatory prostaglandin signaling attenuates excitotoxicity-associated neuronal inflammation and injury. *Neuropharmacology* **149**, 149 (2019). https://doi.org/10.1016/j.neuropharm.2019.02.011
32 Varvel, N. H. *et al.* Preclinical development of an EP2 antagonist for post-seizure cognitive deficits. *Neuropharmacology* **224** (2023). https://doi.org/10.1016/j.neuropharm.2022.109356
33 Rojas, A., Ganesh, T., Lelutiu, N., Gueorguieva, P. & Dingledine, R. Inhibition of the prostaglandin EP2 receptor is neuroprotective and accelerates functional recovery in a rat model of organophosphorus induced status epilepticus. *Neuropharmacology* **93**, 15 (2015). https://doi.org/10.1016/j.neuropharm.2015.01.017
34 Shen, X. *et al.* EZH1 mediates methylation on histone H3 lysine 27 and complements EZH2 in maintaining stem cell identity and executing pluripotency. *Molecular Cell* **32**, 491 (2008). https://doi.org/10.1016/j.molcel.2008.10.016
35 Zhu, Y. *et al.* Ablation of NF1 function in neurons induces abnormal development of cerebral cortex and reactive gliosis in the brain. *Genes & Development* **15**, 859 (2001). https://doi.org/10.1101/gad.862101
36 Basu, T. *et al.* Histone deacetylase inhibitors restore normal hippocampal synaptic plasticity and seizure threshold in a mouse model of Tuberous Sclerosis Complex. *Scientific Reports* **9** (2019). https://doi.org/10.1038/s41598-019-41744-7
37 Cilio, M. R. *et al.* Anticonvulsant action and long-term effects of gabapentin in the immature brain. *Neuropharmacology* **40**, 139 (2001). https://doi.org/10.1016/s0028-3908(00)00103-9
38 Bierkamper, G. G. & Cenedella, R. J. Induction of chronic epileptiform activity in the rat by an inhibitor of cholesterol synthesis, U18666A. *Brain Research* **150**, 343 (1978). https://doi.org/10.1016/0006-8993(78)90285-8
39 Liu, Z. & Holmes, G. L. Basic fibroblast growth factor is highly neuroprotective against seizure-induced long-term behavioural deficits. *Neuroscience* **76**, 1129 (1997). https://doi.org/10.1016/s0306-4522(96)00412-5
40 Applegate, C. D. & Tecott, L. H. Global increases in seizure susceptibility in mice lacking 5-HT2C receptors: a behavioral analysis. *Experimental Neurology* **154**, 522 (1998). https://doi.org/10.1006/exnr.1998.6901
41 Rho, J. M., Kim, D. W., Robbins, C. A., Anderson, G. D. & Schwartzkroin, P. A. Age-dependent differences in fluorothyl seizure sensitivity in mice treated with a ketogenic diet. *Epilepsy Research* **37**, 233 (1999). https://doi.org/10.1016/s0920-1211(99)00068-6
42 Samoriski, G. M. & Applegate, C. D. Repeated generalized seizures induce time-dependent changes in the behavioral seizure response independent of continued seizure induction. *The Journal of Neuroscience: The Official Journal of the Society for Neuroscience* **17**, 5581 (1997).
43 Tipton, A. E. *et al.* Selective Neuronal Knockout of STAT3 Function Inhibits Epilepsy Progression, Improves Cognition, and Restores Dysregulated Gene Networks in a Temporal Lobe Epilepsy Model. *Annals of Neurology* (2023). https://doi.org/10.1002/ana.26644
44 Ahmed, M. M. *et al.* Altered Protein Profiles During Epileptogenesis in the Pilocarpine Mouse Model of Temporal Lobe Epilepsy. *Frontiers in Neurology* **12** (2021). https://doi.org/10.3389/fneur.2021.654606

45 Vishwakarma, S., Singh, S. & Singh, T. G. Pharmacological modulation of cytokines correlating neuroinflammatory cascades in epileptogenesis. *Molecular Biology Reports* **49**, 1437 (2022). https://doi.org/10.1007/s11033-021-06896-8
46 Martín-Suárez, S., Cortes, J. M. & Bonifazi, P. Blockage of STAT3 during epileptogenesis prevents GABAergic loss and imprinting of the epileptic state. *Brain: A Journal of Neurology* (2023). https://doi.org/10.1093/brain/awad055
47 Freeman, L. C. Centrality in social networks conceptual clarification. *Social Networks* **1**, 215-239 (1978).
48 Kupferman, M. E. *et al.* Therapeutic suppression of constitutive and inducible JAK\STAT activation in head and neck squamous cell carcinoma. *Journal of Experimental Therapeutics & Oncology* **8**, 117 (2009).
49 Hussain, S. F. *et al.* A Novel Small Molecule Inhibitor of Signal Transducers and Activators of Transcription 3 Reverses Immune Tolerance in Malignant Glioma Patients. *Cancer Research* **67**, 9630 (2007). https://doi.org/10.1158/0008-5472.can-07-1243
50 Iwamaru, A. *et al.* A novel inhibitor of the STAT3 pathway induces apoptosis in malignant glioma cells both in vitro and in vivo. *Oncogene* **26**, 2435 (2007). https://doi.org/10.1038/sj.onc.1210031
51 Dowty, M. E. *et al.* Preclinical to clinical translation of tofacitinib, a Janus kinase inhibitor, in rheumatoid arthritis. *The Journal of Pharmacology and Experimental Therapeutics* **348**, 165 (2014). https://doi.org/10.1124/jpet.113.209304
52 Meyer, D. M. *et al.* Anti-inflammatory activity and neutrophil reductions mediated by the JAK1/JAK3 inhibitor, CP-690,550, in rat adjuvant-induced arthritis. *Journal of Inflammation (London, England)* **7** (2010). https://doi.org/10.1186/1476-9255-7-41
53 Changelian, P. S. *et al.* Prevention of organ allograft rejection by a specific Janus kinase 3 inhibitor. *Science (New York, N.Y.)* **302**, 875 (2003). https://doi.org/10.1126/science.1087061
54 *UCSC Genome Browser*, <https://genome.ucsc.edu/index.html> (2022).
55 Konze, K. D. *et al.* An orally bioavailable chemical probe of the Lysine Methyltransferases EZH2 and EZH1. *ACS chemical biology* **8**, 1324 (2013). https://doi.org/10.1021/cb400133j
56 Stapels, M. *et al.* Polycomb Group Proteins as Epigenetic Mediators of Neuroprotection in Ischemic Tolerance. *Science Signaling* **3**, ra15 (2010). https://doi.org/10.1126/scisignal.2000502
57 Jenkins, A., Franks, N. P. & Lieb, W. R. Effects of temperature and volatile anesthetics on GABA(A) receptors. *Anesthesiology* **90**, 484 (1999). https://doi.org/10.1097/00000542-199902000-00024
58 Brosnan, R. J. & Thiesen, R. Increased NMDA receptor inhibition at an increased Sevoflurane MAC. *BMC anesthesiology* **12** (2012). https://doi.org/10.1186/1471-2253-12-9
59 Xue, H. *et al.* Sevoflurane post-conditioning alleviates neonatal rat hypoxic-ischemic cerebral injury via Ezh2-regulated autophagy. *Drug Design, Development and Therapy* **13**, 1691 (2019). https://doi.org/10.2147/dddt.s197325
60 Choi, J.-S. *et al.* Upregulation of gp130 and differential activation of STAT and p42/44 MAPK in the rat hippocampus following kainic acid-induced seizures. *Molecular Brain Research* **119**, 10 (2003). https://doi.org/10.1016/j.molbrainres.2003.08.010
61 Wang, H. *et al.* LncRNA-UCA1 inhibits the astrocyte activation in the temporal lobe epilepsy via regulating the JAK/STAT signaling pathway. *Journal of Cellular Biochemistry* **121**, 4261 (2020). https://doi.org/10.1002/jcb.29634
62 Iori, V., Frigerio, F. & Vezzani, A. Modulation of neuronal excitability by immune mediators in epilepsy. *Current Opinion in Pharmacology* **26**, 118 (2016). https://doi.org/10.1016/j.coph.2015.11.002
63 Reetz, O., Stadler, K. & Strauss, U. Protein kinase C activation mediates interferon-β-induced neuronal excitability changes in neocortical pyramidal neurons. *Journal of Neuroinflammation* **11** (2014). https://doi.org/10.1186/s12974-014-0185-4
64 Danis, E. *et al.* Ezh2 Controls an Early Hematopoietic Program and Growth and Survival Signaling in Early T Cell Precursor Acute Lymphoblastic Leukemia. *Cell Reports* **14**, 1953 (2016). https://doi.org/10.1016/j.celrep.2016.01.064
65 Wee, Z. N. *et al.* EZH2-mediated inactivation of IFN-γ-JAK-STAT1 signaling is an effective therapeutic target in MYC-driven prostate cancer. *Cell Reports* **8**, 204 (2014). https://doi.org/10.1016/j.celrep.2014.05.045
66 Kim, E. *et al.* Phosphorylation of EZH2 activates STAT3 signaling via STAT3 methylation and promotes tumorigenicity of glioblastoma stem-like cells. *Cancer Cell* **23**, 839 (2013). https://doi.org/10.1016/j.ccr.2013.04.008

67 Dasgupta, M., Dermawan, J. K. T., Willard, B. & Stark, G. R. STAT3-driven transcription depends upon the dimethylation of K49 by EZH2. *Proceedings of the National Academy of Sciences of the United States of America* **112**, 3985 (2015). https://doi.org/10.1073/pnas.1503152112

68 Cha, T.-L. *et al.* Akt-mediated phosphorylation of EZH2 suppresses methylation of lysine 27 in histone H3. *Science (New York, N.Y.)* **310**, 306 (2005). https://doi.org/10.1126/science.1118947

69 Yan, J. *et al.* EZH2 phosphorylation by JAK3 mediates a switch to noncanonical function in natural killer/T-cell lymphoma. *Blood* **128**, 948 (2016). https://doi.org/10.1182/blood-2016-01-690701

70 Love, M. I., Huber, W. & Anders, S. Moderated estimation of fold change and dispersion for RNA-seq data with DESeq2. *Genome Biology* **15** (2014). https://doi.org/10.1186/s13059-014-0550-8

71 Wolf, F. A., Angerer, P. & Theis, F. J. SCANPY: large-scale single-cell gene expression data analysis. *Genome Biology* **19** (2018). https://doi.org/10.1186/s13059-017-1382-0

72 Assenov, Y., Ramírez, F., Schelhorn, S.-E., Lengauer, T. & Albrecht, M. Computing topological parameters of biological networks. *Bioinformatics (Oxford, England)* **24**, 282 (2008). https://doi.org/10.1093/bioinformatics/btm554

73 Madisen, L. *et al.* A robust and high-throughput Cre reporting and characterization system for the whole mouse brain. *Nature Neuroscience* **13**, 133 (2010). https://doi.org/10.1038/nn.2467

74 Racine, R. J. Modification of seizure activity by electrical stimulation. II. Motor seizure. *Electroencephalography and Clinical Neurophysiology* **32**, 281 (1972). https://doi.org/10.1016/0013-4694(72)90177-0

75 Basu, T. *et al.* Hypothalamic-pituitary-adrenal axis dysfunction worsens epilepsy outcomes and increases SUDEP risk. (Neuroscience, 2022).